Chapter 3: Incorporation of Unnatural Amino Acids into the Binding Site of the M_2 Muscarinic Acetylcholine Receptor

3.1 Introduction

3.1.1 The G-Protein Coupled Receptor Superfamily

More drugs target the G-protein coupled receptor (GPCR) superfamily of proteins than any other protein family[1]. In 2001, 30% of all drugs on the market—and 25% of the top 100 selling drugs—hit GPCRs. Annually, sales for drugs that modulate GPCRs exceed $30 billion[2]. These statistics reflect the diversity of GPCR biology in the cell and the myriad natural ligands that affect GPCRs. Extracellular stimuli as diverse as photons, neurotransmitters, peptides, lipids, and proteases activate GPCR signaling networks involved in processes such as memory, drug addiction, social behavior, three of the five senses (vision, olfaction, and taste), and the regulation of cardiac and pulmonary function[2–4].

As a superfamily, all GPCRs share a topology consisting of seven transmembrane helices (Figure 3.1). The classical model of a GPCR signaling network begins with an extracellular stimulus, such as ligand binding, acting on the resting receptor (Figure 3.1a). A conformational change in the transmembrane helices produces an active conformation, which reorganizes the intracellular face of the GPCR[5]. Heterotrimeric G-proteins—consisting of α, β, γ subunits—bind to the intracellular face of the receptor, which facilitates the exchange of GDP for GTP in the Gα subunit (Figure 3.1b). Upon GTP

binding, the Gα and Gβγ subunits dissociate and affect various downstream cellular targets (Figure 3.1c). Depending on the Gα subfamily, the G-proteins act on different effectors: G_i activates adenyl cyclase (AC), G_q affects phospholipase C (PLCβ), $G_{12/13}$ mediates Rho GTPase activity, and $G_{i/o}$ gates G-protein activated inward rectifying potassium channels (GIRKs) and inhibits AC[6]. G-protein signaling is terminated through the hydrolysis of GTP by the Gα GTPase domain and reassociation of the Gα and Gβγ subunits (Figure 3.1d).

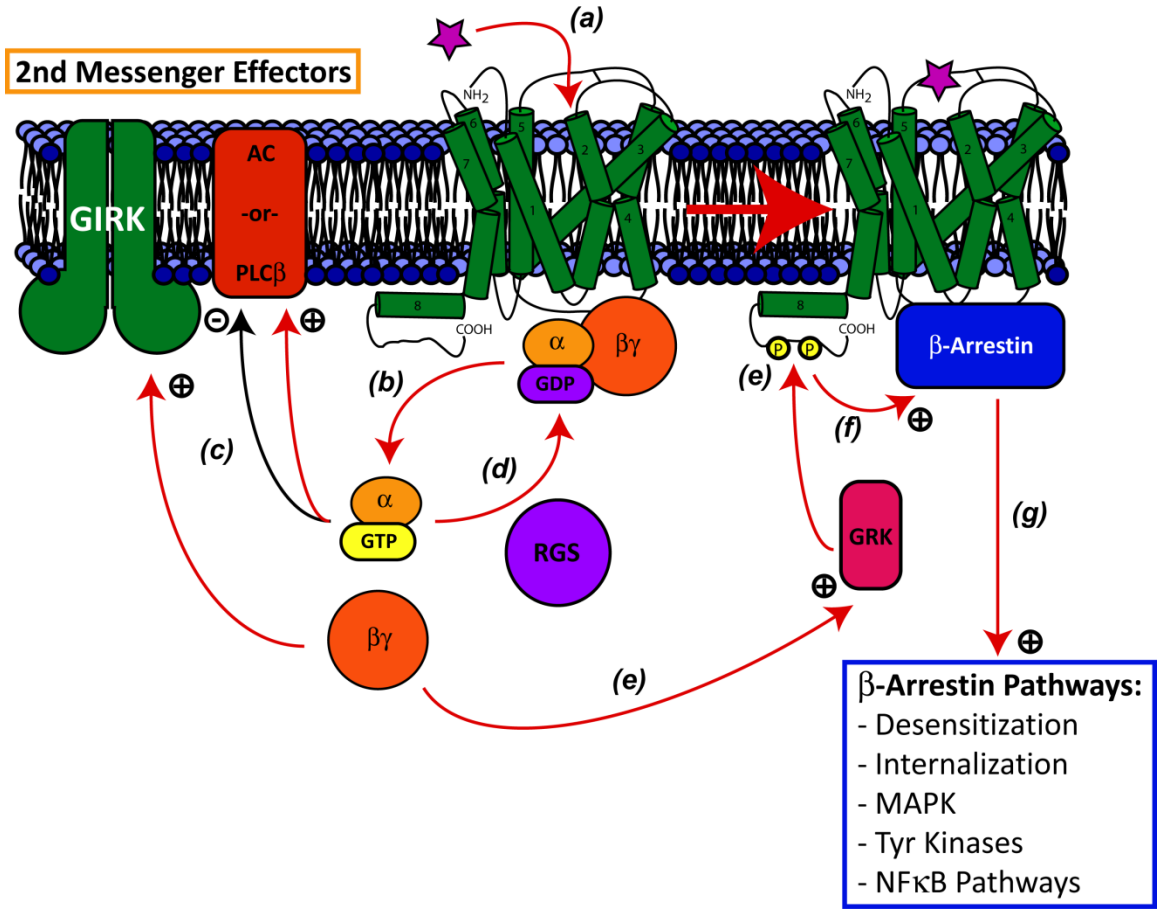

Figure 3.1. GPCR signaling and desensitization pathways

Desensitization of a GPCR signal is a multi-step process that terminates G-protein binding to the receptor[4,7]. In the first step of desensitization, Ser and Thr residues within

the C-terminus of active GPCRs are phosphorylated by GPCR receptor kinases (GRKs). GRKs are activated through interactions with Gβγ (Figure 3.1e). β-arrestin binds to phosphorylated receptor conformations and blocks further G-protein binding (Figure 3.1f). After β-arrestin mediated desensitization, β-arrestin can also interact with other cellular proteins to promote receptor internalization, degradation, and recycling (Figure 3.1g).

GPCR studies in the last decade have revealed a more complex signaling system. The classical image of a GPCR signaling to a specific downstream effector has been modified to allow for GPCRs that can couple to multiple second-messenger pathways [8]. These GPCRs have receptor conformations that can bind multiple subtypes of Gα. Other downstream effectors, not associated with G-protein signaling, can also be modulated through interactions with β-arrestin (Figure 3.1g). Some heterotrimeric G-proteins do not dissociate upon GTP exchange and instead appear to undergo a structural rearrangement between the Gα and Gβγ subunits[9,10]. Receptors and G-proteins also have been found to pre-couple in a signaling complex prior to receptor activation[11–14].

The most significant amendment to the classical GPCR signaling model is the concept of GPCR dimerization[4,15,16]. Researchers who obtained AFM images of rhodopsin dimers have suggested that GPCR dimers are the functional unit of GPCR signaling. According to this model, the G-protein heterotrimer makes contact with both of the monomers, but is only activated by one of the receptors in the dimer[17,18]. While the prevalence of non-rhodopsin GPCR dimers is debated[15], dimer formation has been shown to affect receptor signaling in several different systems. $GABA_B$ receptors must

heterodimerize to produce a competent signaling complex; expression of $GABA_{B1}$ or $GABA_{B2}$ alone does not yield a functional receptor. Heterodimers of opioid receptors are also proposed and believed to affect agonist affinity, pathway signaling, and receptor internalization[19].

GPCRs exhibit other complex pharmacology apart from the effects of dimerization. Different ligands at the same receptor can promote different GPCR-signaling profiles. This phenomenon is called ligand bias[20]. In the parathyroid hormone (PTH) receptor, some peptide agonists trigger G_s-coupled signaling, while other peptides activate both G_q and G_s pathways[20]. Some angiotensin II type 1 (AT_1) and PTH receptor agonists can induce conformations that recruit β-arrestin binding without G-protein activation[20,21]. Finally, there are GPCRs, like the μ-opioid receptor (MOR), that do not desensitize when activated by specific agonists. MOR bound with the natural agonist, enkephalin, desensitizes through the normal β-arrestin mechanism, while morphine bound to MOR does not trigger GRK phosphorylation or β-arrestin binding[22,23].

Inverse agonism is another pharmacological concept associated with GPCRs. An inverse agonist inhibits constitutive activity, which is described as the ability of a receptor to spontaneously adopt an active conformation and couple with G-proteins in the absence of ligand binding. Inverse agonists work by binding to the receptor and stabilizing the resting state of the receptor over the activated state. Because constitutively active mutants (CAMs) in GPCRs are implicated in diseases ranging from cancer to endocrine diseases, like male precocious puberty[24], inverse agonists are an important pharmaceutical target.

3.1.2 The Aminergic Class of GPCRs and Muscarinic Acetylcholine Receptors

Monoamine neurotransmitters, such as dopamine, serotonin, epinephrine, and acetylcholine, can signal through the aminergic class of GPCRs. These receptors belong to the rhodopsin-like family of GPCRs (family A or I) and share many of the structural features found in the rhodopsin crystal structure[25–28]. The receptors have short N-terminal sequences and an eighth amphiphilic helix at the C-terminus that runs parallel to the intracellular side of the membrane bilayer. A conserved disulfide bond connects the first extracellular loop (EL-1), which bridges transmembrane helix 2 (TM2) and TM3, with the second extracellular loop (EL-2), which bridges TM4 and TM5. A recent crystal structure of the β_2 adrenergic receptor (β_2AR) confirms these conserved features[29–31].

Aminergic GPCRs lack large extracellular ligand binding domains, such as those found in metabotropic glutamate receptors (mGluRs). The monoamine ligands instead bind within a shallow crevice created between the seven transmembrane helices (Figure 3.2)[27,32]. There have been many attempts to model the binding sites of aminergic GPCRs[25,33–39], but the low sequence homology between receptors (rhodopsin and the muscarinc receptors only share 16% overall sequence identity and 21% identity within transmembrane regions[36]) has prevented the creation of successful models.

The centerpiece of the aminergic binding site is a highly conserved Asp on TM3, D3.32. (The X.50 numbering convention of Ballesteros[28] will be used throughout this chapter. This convention uses the one-letter amino acid code, the helix number, and a residue index number. To index each residue of a helix, the most conserved residue in

the helix is denoted as 50 and all other residues are numbered N-terminal to C-terminal accordingly. For example, D3.32 refers to an Asp residue on TM3, 18 residues in the N-terminal direction from the highly conserved Arg residue.) Surrounding the conserved D3.32, there is a cluster of aromatic residues reminiscent of the aromatic box found in the binding site of the Cys-loop family of LGICs. The recent β_2AR crystal structure shows the secondary amine of carazolol, an inverse agonist, in close proximity to D3.32 and several aromatic residues[31].

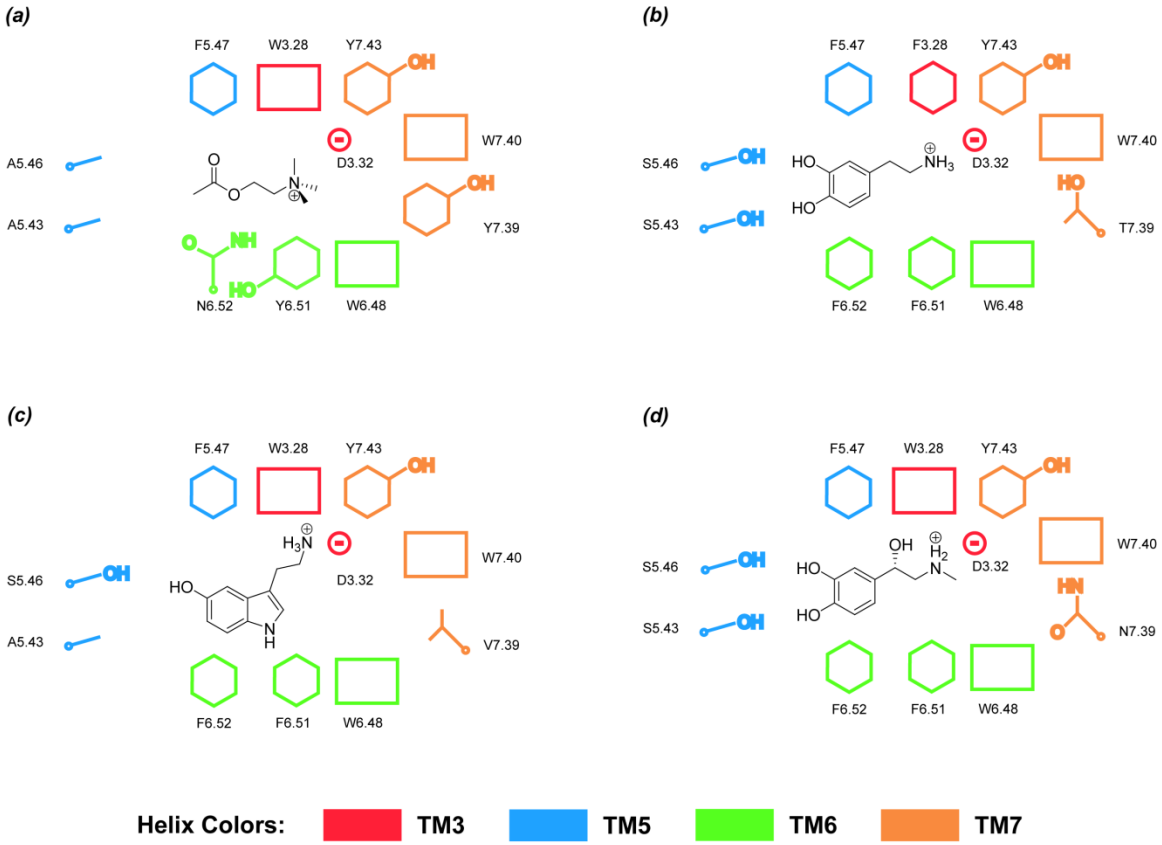

Figure 3.2. Schematic of aminergic GPCR binding sites. ***(a)*** M_2AChR binding site with ACh. ***(b)*** D2R binding site with dopamine. ***(c)*** 5-HT_{2A} binding site with serotonin. ***(d)*** β2AR binding site with epinephrine

Residues that are believed to bind the non-amine end of ligands are also quite conserved. Ser residues on TM5 (S5.46 and S5.43) have been proposed to bind the hydroxyl groups of the catechol containing agonists (dopamine and epinephrine) in the

D_2 dopamine receptor (D_2R) and β_2AR, respectively. In the serotonin 2A receptor (5-$HT_{2A}R$), one of these Ser is an Ala and in the M_2 muscarinic acetylcholine receptor (M_2AChR) both are Ala, which reflects the fact that serotonin only has one hydroxyl group and ACh has none. Position 6.52 also seems to bind non-amine moieties of aminergic agonists. In receptors that have aromatic-based agonists, position 6.52 is conserved as a Phe. This position is an Asn in M_2AChR and is proposed to make a hydrogen bond to the ester moiety of ACh.

There are five sub-types of muscarinic acetylcholine receptor, M_1 through M_5. As a group of GPCRs, the five sub-types of receptors are highly homologous; the group has a 63% sequence identity within the transmembrane region[36]. This high degree of similarity has made the discovery of subtype-specific ligands extremely difficult. As drug targets, the muscarinic receptors are investigated in connection with Alzheimer's disease[40], schizophrenia[41], and smooth muscle disorders, such as overactive bladder, irritable bowel syndrome, and chronic obstructive pulmonary disorder[42].

3.1.3 GIRK 1/4 Readout of M_2AChR

As GPCRs do not produce an easily detectable signal on their own, researchers often use downstream effectors as a readout of GPCR function. In our GPCR experiments described below, we chose to measure M_2AChR activity through GIRK signals. GIRK channels allowed us to utilize electrophysiology as an assay—a technique we have used with the unnatural amino acid methodology for the past decade in our studies of LGICs[23,43–60].

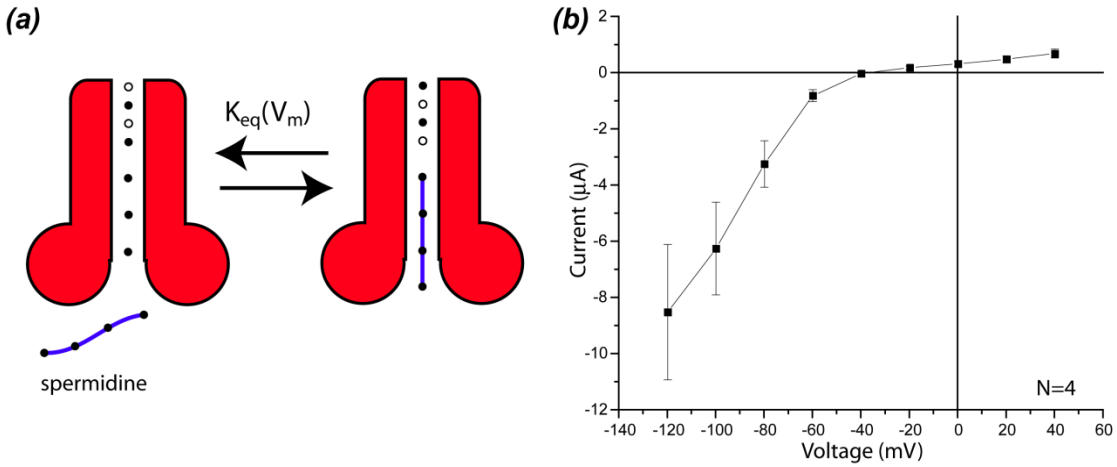

Figure 3.3. Inward rectification. ***(a)*** Schematic for inward rectification mechanism. ***(b)*** Sample IV curve data from GIRK 1/4 channels exhibiting inward rectification

Only M_2AChR and M_4AChR couple to GIRK channels through members of the $G_{i/o}$ family of G-proteins. The other three muscarinic receptors signal through the G_q family and activate PLCβ. Unlike most other downstream effectors of GPCR signaling, GIRK channels are gated through the binding of free Gβγ subunits, not the GTP-bound Gα subunit[61–64]. Four Gβγ subunits are required to gate the channel, one per subunit of the tetrameric ion channel[65,66]. G-protein binding sites have been found on both the N- and C-terminal regions of the GIRK subunits[61,63].

GIRK channels exist as heterotetramers with a X_2Y_2 stoichiometry, where X and Y are two different GIRK subtypes. The two predominant heterotetramers are GIRK1/GIRK2 (GIRK 1/2) and GIRK1/GIRK4 (GIRK 1/4), which are found mainly in the brain and smooth muscle tissue, respectively. Otto Loewi's initial experiments on synaptic transmission showed that a substance released by the vagus nerve slowed the rate of cardiac action potentials. It was later found that this substance was ACh and its target of action was the M_2AChR-GIRK 1/4 signaling system[63,67,68].

As inward rectifying channels, GIRKs do not conduct currents in and out of the cell equally. At depolarized membrane potentials, the channels pass currents inwardly. But, when the cell is hyperpolarized, GIRKs conduct negligible outward currents. At these hyperpolarized membrane potentials, positively charged polyamines inside the cell, like spermidine, bind to the negatively charged intracellular domain of the GIRK and block the channel pore (Figure 3.3a). This intracellular blockage produces an IV relationship that turns over at membrane potentials close to 0 mV (Figure 3.3b)[63].

3.1.4 Goals of Project

As illustrated in the above summary, GPCRs provide many opportunities to explore chemical-level phenomena. Our studies on LGICs have already proven the utility of unnatural amino acid incorporation in analyzing large, complex signaling proteins. We believe that from ligand binding and receptor activation to ligand bias and inverse agonism, the subtlety of unnatural amino acid mutagenesis could provide a new tool in elucidating the structure and function of this significant protein family.

To begin these studies and adapt the unnatural amino acid methodology to the GPCR system, we chose the M_2AChR—a receptor that binds the familiar agonist, ACh—as our initial target. Our first goal was to successfully incorporate unnatural amino acids into the M_2AChR and, using electrophysiological readout from GIRK 1/4 channels, to develop a procedure for assaying receptor function that is robust and reliable. Our second goal was to begin to probe important binding site residues and determine their role in ACh binding. In particular, we wanted to determine whether the quaternary amine

of ACh was bound through a cation-π interaction, as it is in the nicotinic acetylcholine receptor (nAChR)[69].

3.2 Results

3.2.1 Electrophysiology of the M_2AChR-GIRK 1/4 System

Figure 3.4 illustrates the basic procedure we used in our M_2AChR-GIRK 1/4 assays. Because GIRKs only conduct inward currents, against the potassium concentration gradient, a ringer solution with a high potassium concentration must be used to produce significant current magnitudes. We chose to use a ringer solution that is the same as ND96, but has a potassium concentration of 24 mM (ND96 potassium concentration of 2 mM). This concentration of potassium generated currents of sufficient magnitude and was tolerated well by the cells.

To assay the response of the M_2AChR to a given dose of ACh, our experiments began by voltage clamping the cell at -60 mV. Higher currents can be produced if more negative holding potentials are used[70], but we found that these higher holding potentials lead to more extensive cell death through the course of an experiment. After an initial pre-wash of ND96 to determine a baseline current level (Figure 3.4a), we switched to the high-potassium ringer. Upon switching to the high-potassium ringer, a basal potassium current was generated due to the presence of free Gβγ inside the cell[66,71]. After 50 s, this standing current began to level off. A dose of ACh in the high-potassium ringer was then applied to the cell for 15 s. Drug was washed out of the chamber through a two-phase

wash protocol; the initial phase involved washing with the high-potassium ringer and the final phase consisted of a longer wash with ND96.

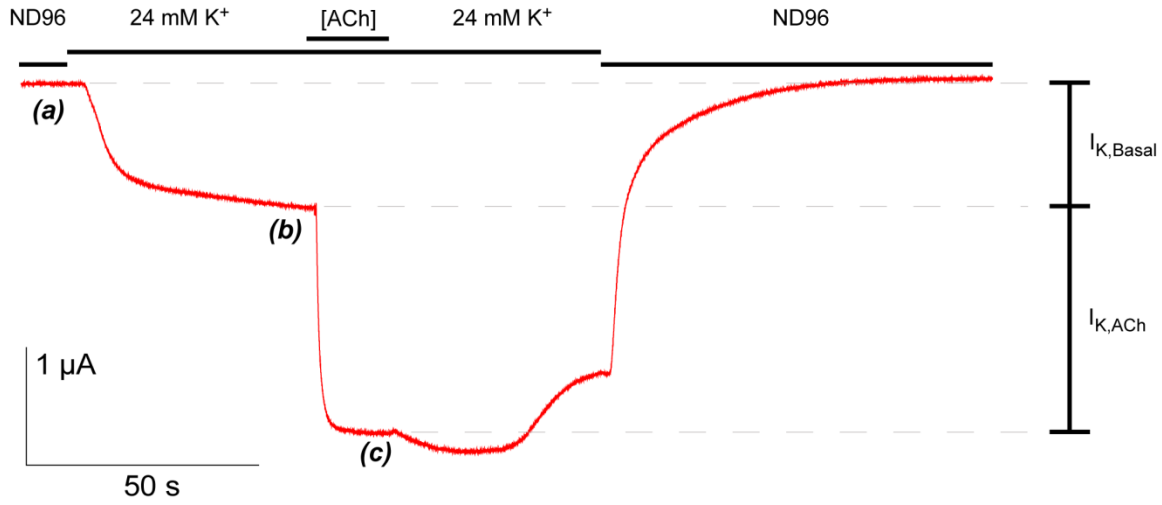

Figure 3.4. Example of a GPCR electrophysiology experiment. ND96 ringer solution has a potassium concentration of 2 mM. ACh is applied in the presence of the high-potassium ringer. $I_{K,\ Basal}$ is defined as the current difference between ***(b)*** and ***(a)***; subtraction of ***(b)*** from ***(c)*** yields $I_{K,\ ACh}$

For the rest of this chapter, we will refer to two current measurements frequently. $I_{K,Basal}$ refers to the basal potassium current produced by free Gβγ and is measured as the difference between the current level at the end of the high-potassium pre-wash (Figure 3.4b) and the initial baseline current in ND96 (Figure 3.4a). $I_{K,ACh}$ is defined as the ACh-induced current and is measured as the difference between the current at the end of the 15 s drug application (Figure 3.4c) and at the end of the high-potassium ringer pre-wash (Figure 3.4b).

The above experimental procedure was successful in producing robust M_2AChR-GIRK 1/4 signals, but the resulting data was highly variable. In the following sections, we will discuss the current and, especially, EC_{50} data variability that we observed. We will also describe how this system was optimized to yield reproducible data.

3.2.2 Co-Injection of Gα mRNA Blocks $I_{K,Basal}$

Our first attempt to eliminate a possible source of variability in the GPCR assay was to control $I_{K,Basal}$. We believed that because we could not control the level of free Gβγ in the cell, basal current levels might fluctuate greatly and affect the reliability of our data. To control free Gβγ levels in the cell, we injected Gα mRNA with the mRNA for M_2AChR and GIRK 1/4. The extra Gα proteins in the cell would bind to any free Gβγ subunits. Previous experiments had shown that co-injecting Gα mRNA produced lower or negligible basal current levels[66,71].

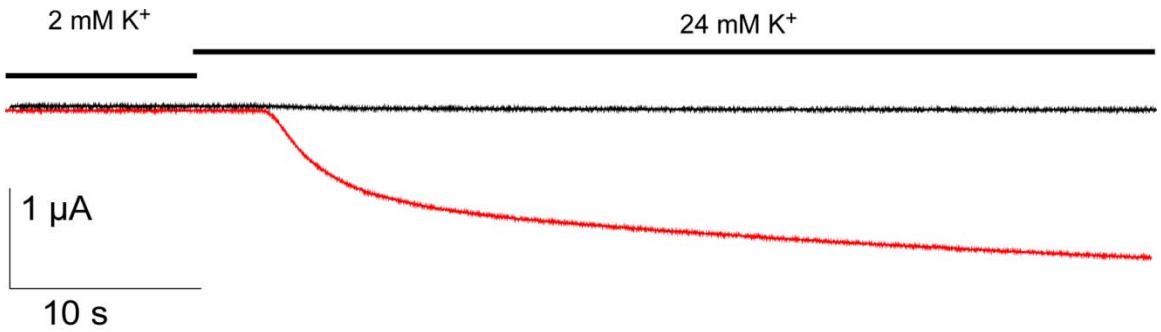

Figure 3.5. Example of $I_{K,\ Basal}$ suppression through injection of Gα mRNA. Black trace is M_2AChR / GIRK 1/4 system with 10 ng $G\alpha_{oA}$ mRNA, while red trace is the system without additional Gα mRNA.

We decided to use $G\alpha_{oA}$ mRNA because a previous study showed that co-injections with it not only produced the lowest $I_{K,Basal}$, but also exhibited higher $I_{K,ACh}$ when compared to injections of other $G_{i/o}$ mRNAs[66]. In our experiments, co-injection of 10 ng of $G\alpha_{oA}$ mRNA significantly decreased $I_{K,Basal}$ by 86% from 0.7 μA to 0.1 μA (Figures 3.5 and 3.6a). $I_{K,ACh}$ also increased by 65% from 2.0 μA to 3.3 μA (Figure 3.6a). Reducing the amount of $G\alpha_{oA}$ mRNA injected from 10 ng to 2 ng also produced a significant increase in $I_{K,ACh}$ (Figure 3.6b). We therefore decided to proceed by co-injecting 2 ng of $G\alpha_{oA}$ mRNA in subsequent experiments.

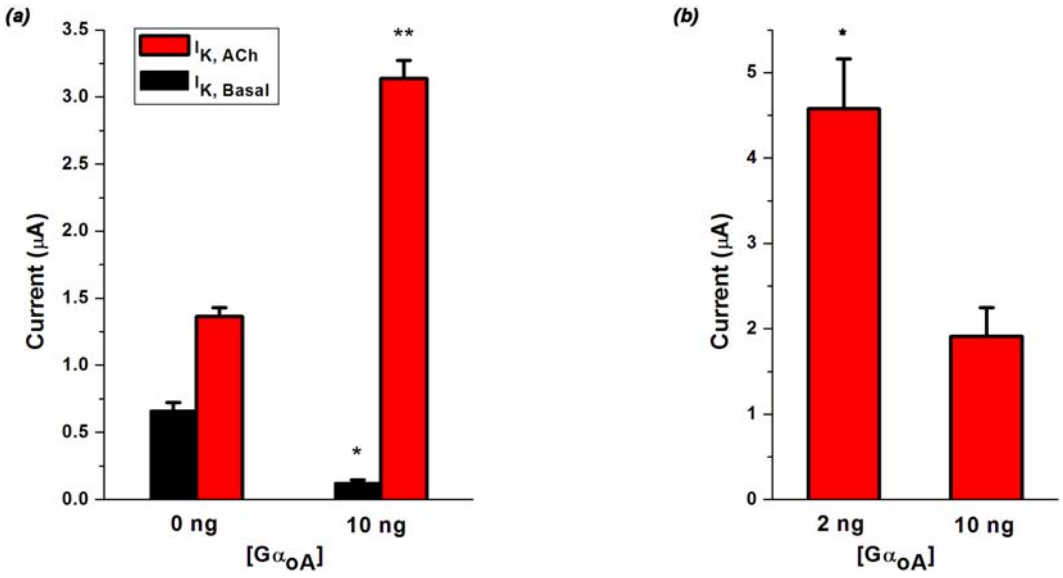

Figure 3.6. Experiments with $G\alpha_{oA}$ mRNA injections. ***(a)*** Co-injection of 10 ng of $G\alpha_{oA}$ mRNA decreases $I_{K, Basal}$ from 0.7 μA to 0.1 μA, while increasing $I_{K,ACh}$ from 2.0 μA to 3.3 μA. N = 6 and N = 7 for the 0 ng and 10 ng conditions, respectively. ***(b)*** Decreasing $G\alpha_{oA}$ mRNA from 10 ng to 2 ng, enhanced $I_{K, ACh}$ by 142% (1.9 μA to 4.6 μA). N = 20 and N= 9 for the 2 ng and 10 ng conditions, respectively. Error bars are SEM. * *t*-test $p = 0.01$; ** *t*-test $p = 0.001$

3.2.3 RGS4 and Current Trace Kinetics

It has been known in the M_2AChR-GIRK 1/4 literature that $I_{K,ACh}$ trace kinetics do not resemble native kinetics in cardiac cells without the injection of an additional component[72]. This additional component is the regulator of G-protein signaling 4 (RGS4). Proteins belonging to the RGS family all act as G-protein-activating proteins (GAPs) by accelerating the kinetics of GTP hydrolysis in the Gα GTPase domain. RGS4 proteins bind Gα and stabilize the switch I and II regions of the GTPase domain, which contain the domain's catalytic residues.

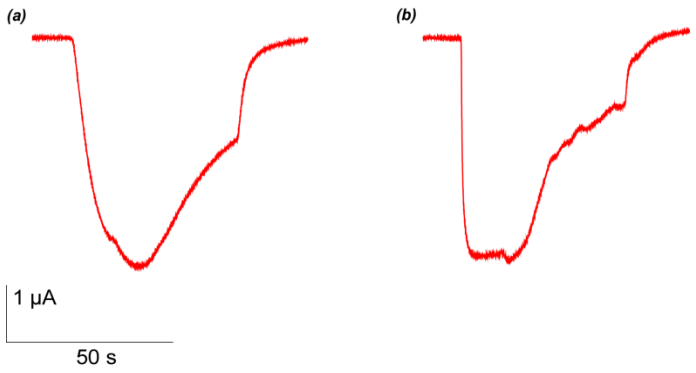

Figure 3.7. RGS kinetic effect. 0.5 ng M_2AChR / 10 ng GIRK 1/4 co-injected with 0 ng ***(a)*** and 10 ng RGS4 ***(b)***. RGS4 mRNA co-injection increases both activation and deactivation kinetics.

The electrophysiological consequence of adding RGS4 to the cell is faster deactivation kinetics in $I_{K,ACh}$ traces (Figure 3.7). Also, it has been observed that RGS4 co-injection increases activation kinetics (Figure 3.7). Researchers have proposed that RGS4 not only acts as a GAP, but also serves as scaffolding for a signaling complex between the GPCR, G-protein, and GIRK channel[65,66]. In this model, activation kinetics are thought to be increased through maintaining the signaling partners in close proximity.

For our experiments, we sought uniform traces that reached a maximum $I_{K,ACh}$ level quickly and, therefore, we experimented with RGS4 mRNA injections. We compared the effects of injecting 10 ng of RGS4 mRNA at two different times, 48 hrs and 24 hrs, prior to recording. Injection 24 hrs before recording yielded more uniform accelerated kinetics than 48 hr injection. Throughout the rest of this chapter, all experiments described will involve a 10 ng injection of RGS4 mRNA 24 hours prior to recording.

3.2.4 Dose-Response Relationships for Conventionally Expressed M_2AChRs

After diminishing $I_{K,Basal}$ and establishing proper accelerated RGS kinetics, we sought to determine an ACh dose-response relationship for M_2AChR using conventional expression of the receptor. One issue we were particularly concerned with when performing these experiments was avoiding spare receptor conditions. When GPCRs significantly outnumber their downstream effectors, the signaling system is described as having spare receptors (Figure 3.8a). This disparity between GPCR and downstream effector numbers creates a situation where the downstream signal is saturated before the receptor binding site becomes saturated. Essentially, the signal saturates prematurely. As a consequence the dose-response relationship shifts and produces a lower EC_{50} value (Figure 3.8b). To avoid spare receptors when we performed our experiments, we injected a series of different GIRK : M_2AChR mRNA ratios and monitored for shifts in EC_{50}.

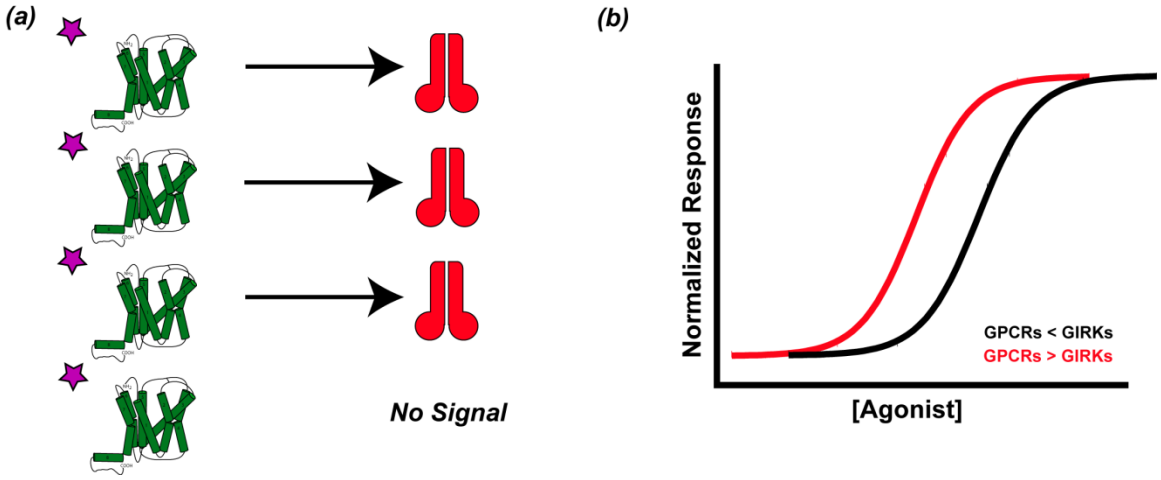

Figure 3.8. Scheme for spare receptors. ***(a)*** When GPCRs outnumber Girk channels, the downstream signal is saturated before the receptor binding site is saturated by drug. ***(b)*** Spare receptors (red) produce a shift in the dose-response relationship from the actual curve (black) towards lower EC_{50} values.

(Throughout the rest of this chapter, we will be discussing two different types of EC_{50} values. The first value is the EC_{50} obtained when each cell's dose-response

relationship data is fit to the Hill equation. This value will be referred to as the cell EC_{50}, or cEC_{50}. The second value is our standard definition, where the responses to each drug dose are averaged across all cells and these averaged responses are fit to the Hill equation. This value will be referred to simply as EC_{50}. The two values, although similar, are not identical.)

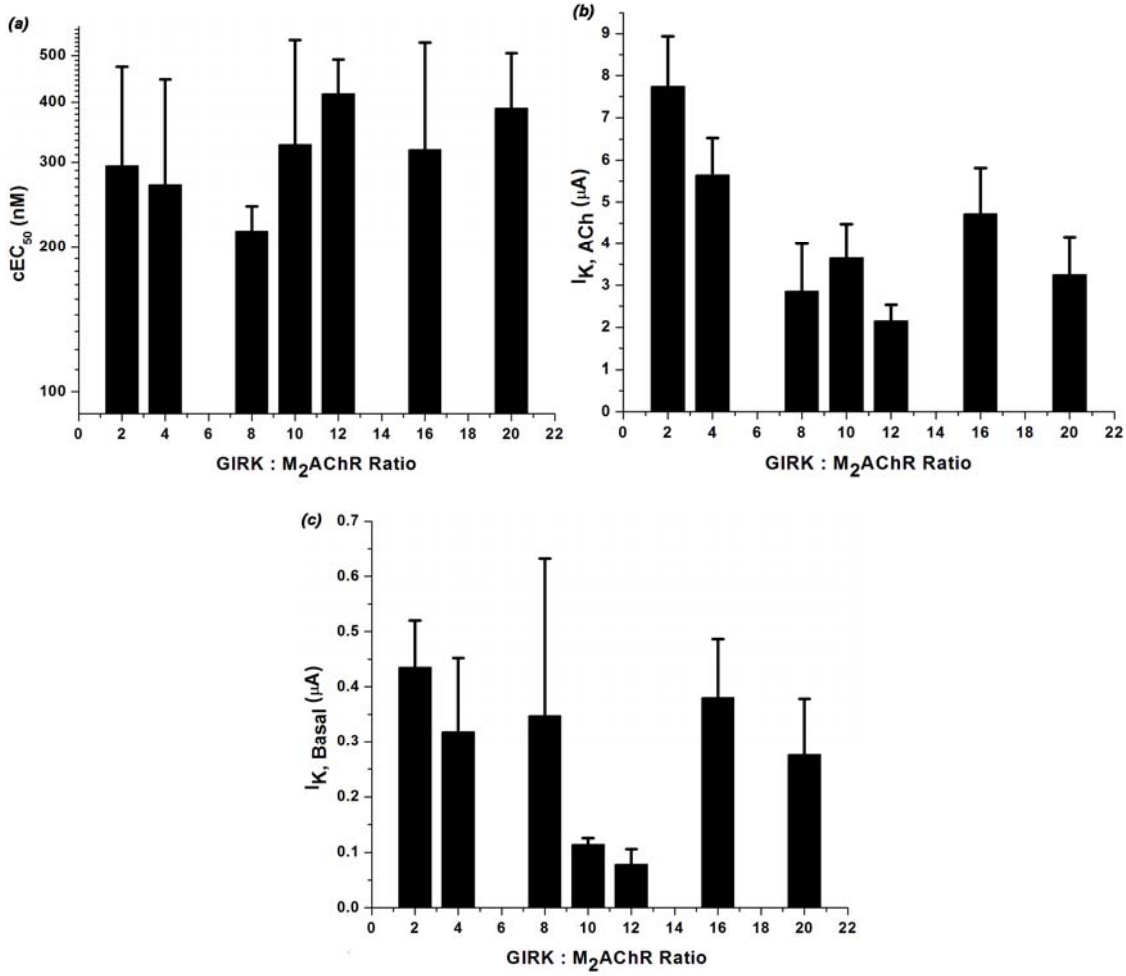

Figure 3.9. GIRK:M_2AChR mRNA injection ratio comparisons of cEC_{50} ***(a)***, $I_{K,ACh}$ ***(b)***, and $I_{K,Basal}$ ***(c)***. One-way ANOVA test for differences between mRNA ratio groups show no significant difference for any of the three measurements. (cEC_{50} F-value = 0.77; df = 6, 50; *p*-value = 0.6. $I_{K,ACh}$ F-value = 2.04; df = 6, 50; *p*-value = 0.8. $I_{K,Basal}$ F-value = 0.71; df = 6, 50; *p*-value = 0.6.) Cell counts for the conditions are N = 22, 16, 3, 4, 4, 3, and 5 for the 2, 4, 8, 10, 12, 16, and 20 Girk:M_2AChR mRNA ratio conditions, respectively. Error bars are standard deviation ***(a)*** and SEM ***(b)*** and ***(c)***.

The different injection ratios had no significant effect on current levels or cEC_{50} values (Figure 3.9). The dose-response relationship remained the same from GIRK : M_2AChR mRNA ratios of 2:1 up through 20:1. We therefore concluded that we were not experiencing spare receptors in these experiments. When data from all 57 cells were combined, the EC_{50} for conventionally expressed M_2AChR was 250 ± 10 nM ACh (Figure 3.10).

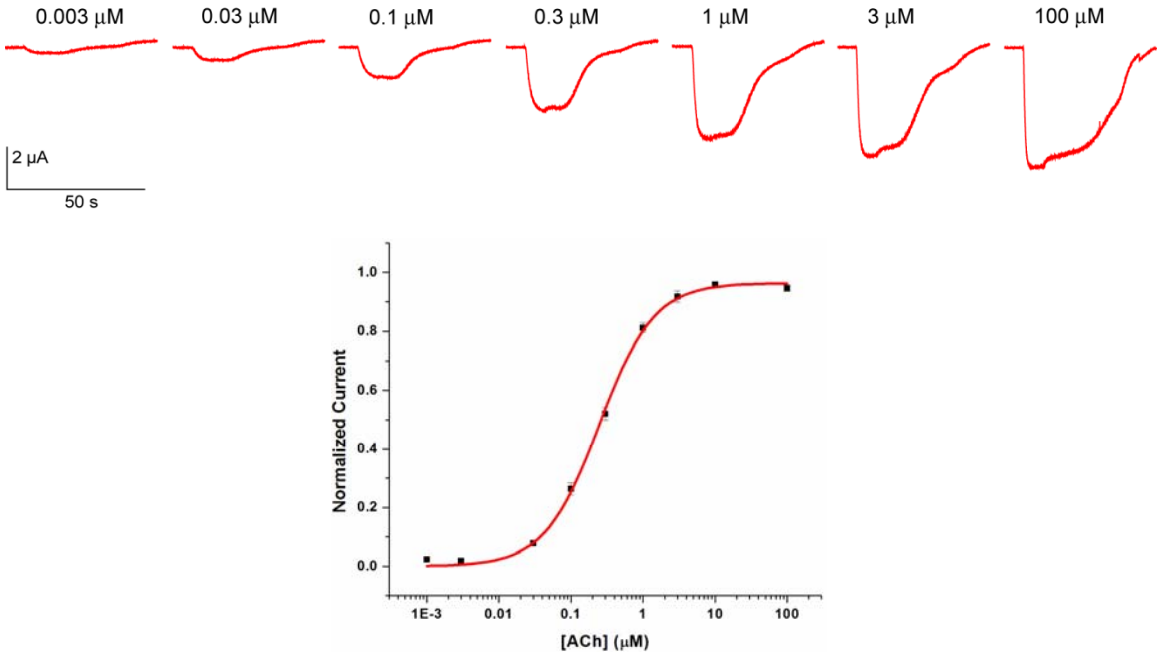

Figure 3.10. Conventional M_2AChR / GIRK 1/4 ACh dose-response experiment. *Top*: Sample $I_{K,ACh}$ traces with ACh dose concentrations. *Bottom*: Dose-response curve for N = 57 cells that were injected with varying GIRK 1/4: M_2AChR mRNA ratios and 2 ng $G\alpha_{oA}$ mRNA. Curve fit parameters: EC_{50} = 250 ± 10 nM; n_H = 1.2 ± 0.1

3.2.5 Wild-Type Recovery of M_2AChR

Once we had assured ourselves that we had established an accurate dose-response relationship for wild-type M_2AChR through conventional expression, we next attempted to assay a wild-type receptor through nonsense suppression. In this wild-type recovery

experiment, a stop codon was placed at a specific site within the M_2AChR gene and THG73 tRNA ligated with the wild-type amino acid was injected into the cell to re-establish the wild-type protein. Following what we had learned in our conventional experiments, these nonsense suppression experiments included co-injection of $G\alpha_{oA}$ mRNA at the same time as the mutant M_2AChR and GIRK 1/4 mRNA and a subsequent injection of RGS4 mRNA 24 hours before recording.

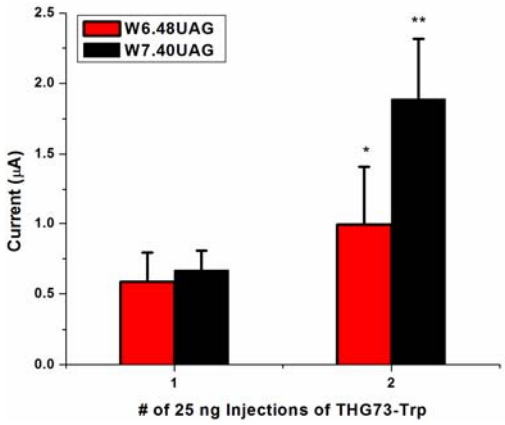

Figure 3.11. $I_{K,ACh}$ and number of suppressor tRNA injections. 20.5.2 W7.40UAG (black) and 20.5.0 W6.48UAG (red) conditions were used with 1 or 2 injections of 25 ng THG73-Trp. $I_{K,ACh}$ for the 1 injection conditions were 0.7 μA and 0.6 μA for the W7.40 and W6.48 conditions, respectively. A second injection of tRNA increased currents to 1.9 μA and 1.0 μA in the W7.40 and W6.48 experiments, respectively. (* *t*-test *p*-value = 0.02, with N = 9 for both injection conditions; ** *t*-test *p*-value = 0.03, with N = 9 for the 1 injection and N = 6 for the 2 injection conditions.) Error bars are SEM

(For the rest of this chapter, we will refer to suppression experiment conditions through a X.Y.Z triplet, where X is the amount of mutant M_2AChR mRNA, Y is the amount of mRNA for each GIRK subunit, and Z is the amount of $G\alpha_{oA}$ mRNA injected. In every case, 10 ng of RGS4 mRNA was injected 24 hrs before recording. As an example, 20.5.2 refers to the experiment where 20 ng of the M_2AChR mRNA, 5 ng each of GIRK1 and GIRK4 mRNA, and 2 ng of $G\alpha_{oA}$ mRNA were injected. A given nonsense suppression mutation will be described in the following manner: the site of stop codon mutation will be written with the X.50 numbering convention and the amino acid

incorporated at that position will be written with the three-letter amino acid code. W7.40Trp refers to an experiment at position W7.40, where Trp was incorporated at the position through nonsense suppression.)

In an attempt to produce optimal expression levels, we tried one and two injections of suppressor tRNA. The first injection always occurred along with the M_2AChR, GIRK, and Gα mRNAs 48 hrs prior to recording. A second injection was performed in some cells along with the RGS4 mRNA injection 24 hrs before assaying. We performed this injection study on two different mutants, W6.48Trp with injection conditions 20.5.0 (20.5.0 W6.48Trp) and W7.40Trp with injection conditions 20.5.2 (20.5.0 W7.40Trp). In both cases, a second injection of tRNA led to larger $I_{K,ACh}$ (Figure 3.11). These larger currents were interpreted as greater expression efficiency of the M_2AChR protein. We therefore adopted double tRNA injections as part of our GPCR nonsense suppression methodology.

Our initial nonsense suppression experiments also involved varying the amounts of mutant M_2AChR mRNA. We found that 20 ng of UAG mutant mRNA produced the most reliable expression of receptors and adequate $I_{K,ACh}$ levels. Because expression of proteins with incorporated unnatural amino acids is limited by the amount of tRNA we inject into the cell, we were not concerned about spare receptors. The low expression efficiency of nonsense suppression would ensure that M_2AChR expression levels never outpaced GIRK expression levels. GIRK mRNA injection amounts were also kept at 5 ng to further avoid spare receptors. At the end of these initial experiments, we arrived at the 20.5.2 suppression conditions with double tRNA injections. We then began to collect

ACh dose-response relationship data for wild-type recovery and unnatural amino mutant receptors.

3.2.6 cEC_{50} Variability in Nonsense Suppression M_2AChR Experiments

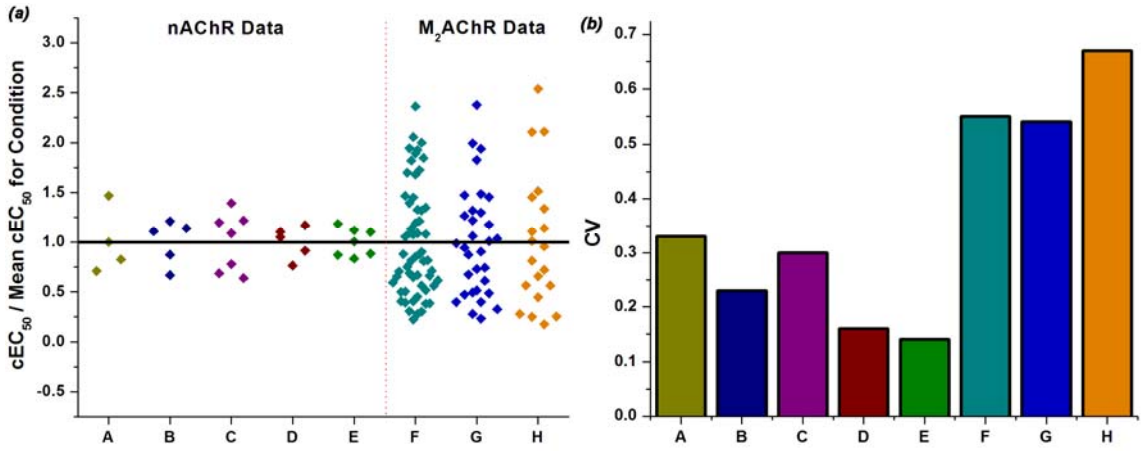

Figure 3.12. Cell-to-cell variability of nAChR and M_2AChR suppression data. ***(a)*** cEC_{50} values normalized to the mean EC_{50} for the condition. ***(b)*** Bar chart showing the CV values for the conditions in ***(a)***. M_2AChR suppression data has greater than twice the CV value of nAChR data (left side of ***(a)***). A: nAChR, D89Asp ACh data (CV = 0.33); B: nAChR, D89Akp ACh data (CV = 0.23); C: nAChR, D89Nha ACh data (CV = 0.30); D: nAChR, D89Akp Epi data (CV = 0.16); E: nAChR D89Nha Epi Data (CV = 0.14); F: M_2AChR conventional WT (CV = 0.55); G: M_2AChR 20.5.2 W7.40Trp (CV = 0.54); H: M_2AChR 20.5.2 W7.40F_1Trp (CV = 0.68)

Analysis of our dose-response relationship data for the first series of experiments with the 20.5.2 suppression conditions revealed two different types of variability in cEC_{50} values. These first experiments involved the wild-type recovery mutant, W7.40Trp, and the incorporation of 5-F-Trp (F_1Trp) at W7.40, W7.40F_1Trp. The conventional M_2AChR data set and the two mutant data sets all exhibited twice the cell-to-cell cEC_{50} variability as nAChR data when measured by the coefficient of variation (CV; Figure 3.12). The coefficient of variation is defined as the ratio of the standard deviation to the mean of a population. This variation can also be visualized by normalizing the cEC_{50} values to the mean cEC_{50} for a specific condition and observing the spread of data from 1 (Figure

3.12a); the standard deviation of the transformed data is equal to the CV of the non-transformed data.

With higher levels of cell-to-cell variability, we wondered what kind of shifts in cEC_{50} or EC_{50} we could interpret statistically. To address this concern, we derived a formula for the student's *t*-test in terms of CV and a z-fold shift in cEC_{50} (details in Appendix B). This formula allowed us to determine what z-fold shifts in EC_{50} could be significantly differentiated when the data had high CVs. When studying other receptors, we have not attempted to physically interpret 3-fold shifts and below. For data with a CV of 0.25 (nAChR data variability) or a CV of 0.5 (M_2AChR data variability), 3-fold shifts are significantly different at a > 99% confidence level. 3.5-fold shifts in EC_{50} values can be significantly differentiated in populations with a CV of 1.0. Also, increasing the number of cells collected for each condition increases the statistical significance of small cEC_{50} shifts. Because cEC_{50} values are similar to EC_{50} values, we assumed that significant shifts in cEC_{50} data would produce significant shifts in EC_{50} values. Therefore, the level of cell-to-cell variability of data observed in our M_2AChR conventional and suppression experiments were not so high as to prevent us from interpreting EC_{50} shifts that we have considered to be significant in previous LGIC experiments.

But another type of data variability we observed in our nonsense expression experiments was not manageable. Compared to our conventional expression experiments, the batch-to-batch variability of cEC_{50}s was high (Figure 3.13); we define batch-to-batch variability as the variation in the mean cEC_{50} for a batch of cells injected under the same conditions. The batch-to-batch CV of the 20.5.2 W7.40F_1Trp nonsense

suppression experiment conditions was twice that of the conventional expression experiment (Figure 3.13b).

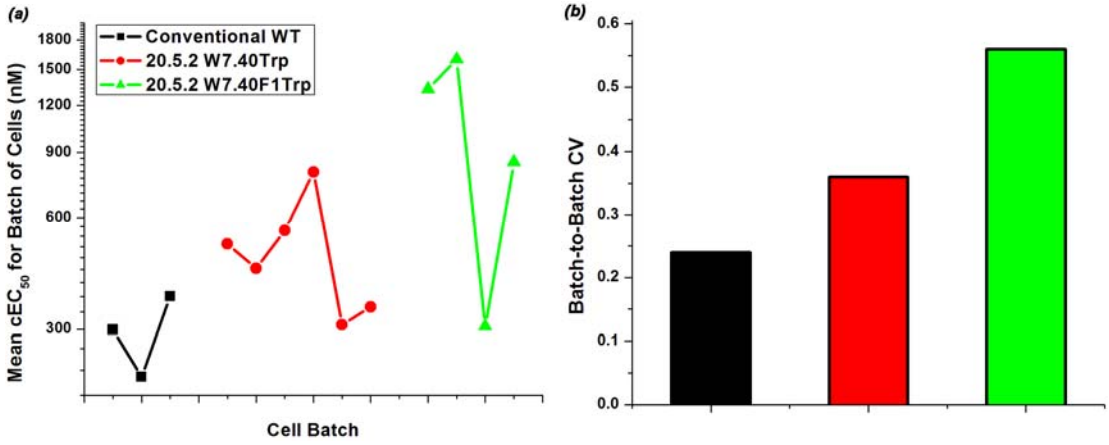

Figure 3.13. Comparison of batch-to-batch variability for conventional and suppression M_2AChR data. ***(a)*** Mean cEC_{50} values for each cell batch in a given expression condition are plotted. ***(b)*** The batch-to-batch CV values for batch cEC_{50}s are shown. Condition colors match those in ***(a)***. Batch-to-batch CVs are 0.24, 0.36, and 0.56 for the conventional wild type, 20.5.2 W7.40Trp, and 20.5.2 W7.40F_1Trp conditions, respectively

Table 3.1. cEC_{50} values for conventional and suppressed wild-type experiments based on $I_{K,ACh}$[a]

	EC_{50}	**n_H***	**N**
Conventional WT (all cells)	250 ± 12	1.2 ± 0.1	57
Conventional WT ($I_{K,ACh}$ > 2 μA)	230 ± 8	1.2 ± 0.04	40
Suppressed WT (all cells)	440 ± 10	1.1 ± 0.03	30
Suppressed WT ($I_{K,ACh}$ > 2 μA)	300 ± 10	1.1 ± 0.1	16

[a]EC_{50} (nM) and n_H values are ± SEM.

3.2.6.1 Gα and Higher cEC_{50} Values

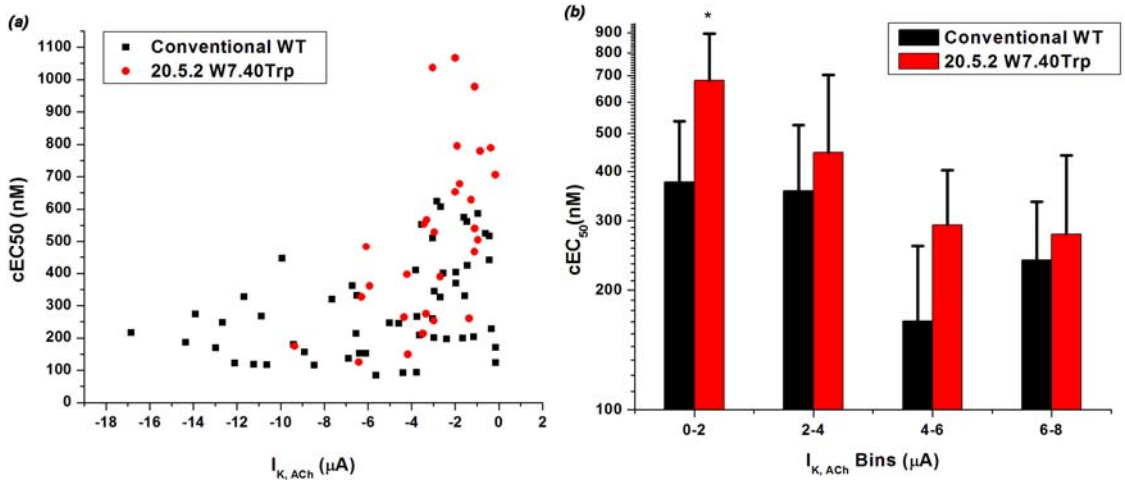

Figure 3.14. Suppression M_2AChR experiments exhibit higher cEC_{50} values in cells with low $I_{K,ACh}$. ***(a)*** When $I_{K,ACh}$ is plotted with cEC_{50}, conventional and suppressed wild-type data diverge most for cells with $I_{K,ACh}$ < 2 μA. ***(b)*** Cell data are placed in 2 μA current bins. * *t*-test *p*-value < 0.001. In the four current bins, N = 15 and 13 for the 0 to 2 μA bin, N = 14 and 9 for the 2 to 4 μA bin, N = 4 and 4 for the 4 to 6 μA bin, and N = 7 and 4 for the 6 to 8 μA bin, for the conventional and suppressed conditions, respectively. Error bars are standard deviations

In addition to the batch-to-batch variability of the nonsense suppression data, we also observed an upward shift in the EC_{50} value for the entire 20.5.2 W7.40Trp data set (440 nM) compared to the conventional wild-type experiment (240 nM; Table 3.1). To try to remedy this elevated wild-type recovery EC_{50} and, hopefully, the batch-to-batch data variability, we began to search for trends between cEC_{50} and other properties of our M_2AChR-GIRK 1/4 signaling system. When we analyzed the relationship between $I_{K,ACh}$ and cEC_{50}, we found that cells from our nonsense suppression experiments with low $I_{K,ACh}$ had higher cEC_{50} values on average than cells with equivalent current levels in the conventional expression experiments (Figure 3.14). In fact, separating cells from both conventional and 20.5.2 W7.40Trp experiments into 2 μA bins showed that the two data sets only differed significantly in the 0 to 2 μA current bin (Figure 3.14b). If cells with $I_{K,ACh}$ less than 2 μA were removed from both data sets, the difference between the two

EC_{50} values narrowed (230 nM and 300 nM for the conventional and nonsense suppression experiments, respectively; Table 3.1). We concluded that low levels of M_2AChR expression in the nonsense suppression experiments, which would lead to low $I_{K,ACh}$ levels, were producing abnormally shifted ACh dose-response relationships.

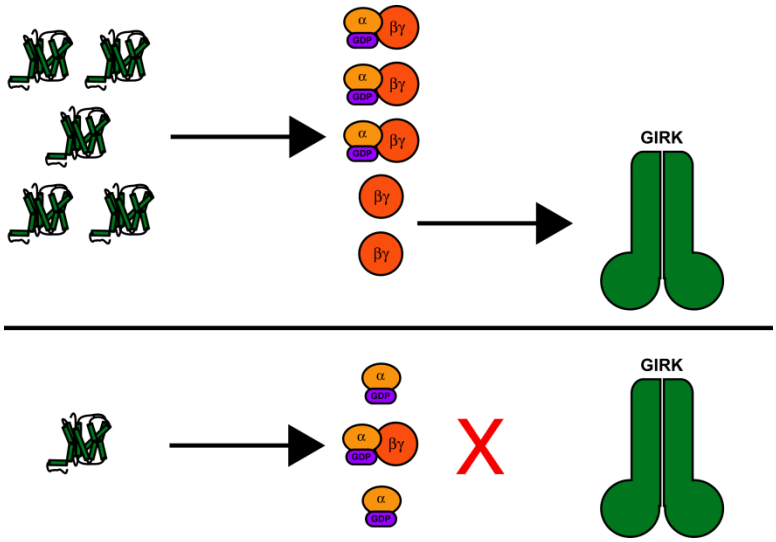

Figure 3.15. Possible explanation of low $I_{K,ACh}$ / high cEC_{50} phenomenon. Co-injection of $G\alpha_{oA}$ mRNA produces greater amounts of $G\alpha_{oA}$ protein that can block free $G\beta\gamma$. In cells with average-to-high GPCR expression (*top*), higher amounts of $G\alpha_{oA}$ do not affect GPCR-mediated free $G\beta\gamma$ signaling to downstream GIRK channels. But, if GPCR expression is low (*bottom*) and low amounts of GPCR-mediated free $G\beta\gamma$ are produced, then the higher amounts of $G\alpha_{oA}$ will block free $G\beta\gamma$ and a higher dose of drug will be required to produce the same level of GIRK signal

One possible explanation for this connection between expression levels and dose-response relationships is the injection of $G\alpha_{oA}$ mRNA. Nonsense suppression produces lower levels of receptor expression than conventional expression methods. Lower receptor expression would produce a lower flux of free $G\beta\gamma$ subunits in response to ACh application. With the injection of $G\alpha_{oA}$ mRNA, there would also be an increased level of free $G\alpha$ inside the cell, which could bind to free $G\beta\gamma$ subunits and prematurely terminate M_2AChR-GIRK signaling (Figure 3.15). Therefore, a higher dose of ACh would be needed in low-expressing cells to produce the equivalent amount of signal as in normally

expressing cells. Such a phenomenon would shift the dose-response relationship to higher cEC_{50} values.

Table 3.2. EC_{50} values for conventional and suppressed wild-type experiments with varying amounts of co-injected $G\alpha_{oA}$ mRNA[a]

	EC_{50}	**n_H^***	**N**
Conventional WT (2 ng $G\alpha_{oA}$)	250 ± 10	1.2 ± 0.1	57
Conventional WT (0 ng $G\alpha_{oA}$)	240 ± 30	0.8 ± 0.1	9
Suppressed WT (2 ng $G\alpha_{oA}$)	440 ± 10	1.1 ± 0.03	30
Suppressed WT (1 ng $G\alpha_{oA}$)	400 ± 10	0.9 ± 0.03	20
Suppressed WT (0 ng $G\alpha_{oA}$)	290 ± 30	0.8 ± 0.1	17

[a]EC_{50} (nM) and n_H values are ± SEM.

To test this hypothesis and reduce data variability, we performed a series of W7.40Trp experiments where we reduced the amount of $G\alpha_{oA}$ mRNA injected and monitored the change in mean cEC_{50}. Cells with 0 ng of injected $G\alpha_{oA}$ mRNA had cEC_{50}s that were not significantly different from the conventional expression experiments and significantly lower than cells with 2 ng or 1 ng of $G\alpha_{oA}$ mRNA (Figure 3.16a). When all of the cells from each condition were pooled together, the EC_{50} for 20.5.0 W7.40Trp was 290 nM, similar to the conventional wild-type EC_{50} of 240 nM (Table 3.2). To ensure that removing $G\alpha_{oA}$ from conventional expression experiments did not change the dose-response relationship, we determined the EC_{50} for a $G\alpha$-free conventional expression experiment and found no difference from the previous EC_{50}.

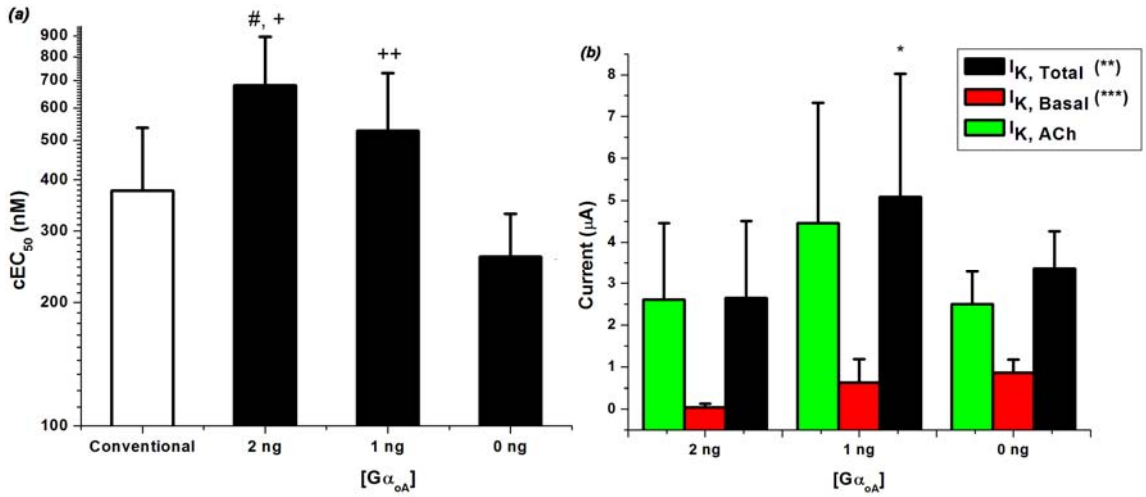

Figure 3.16. $G\alpha_{oA}$ / cEC_{50} mRNA experiments. ***(a)*** Varying the amount of $G\alpha_{oA}$ mRNA injected in suppression experiments affects cEC_{50} values. + *t*-test for comparison of 2 ng to 0 ng, *p*-value = 0.002; ++ *t*-test comparison of 1 ng to 0 ng, *p*-value = 0.02; # comparison of 2 ng to conventional, *p*-value = 0.002. ***(b)*** Lowering $G\alpha_{oA}$ mRNA amounts also affected $I_{K,Total}$ and $I_{K,basal}$ levels. *** One-way ANOVA test for $I_{K,Basal}$ differences between the three injection conditions, F-value = 56.34, df = 2, 62, and *p*-value << 0.001. ** One-way ANOVA test for $I_{K,Total}$ differences between the three injection conditions, F-value = 8.03, df = 2, 62, and *p*-value < 0.001. * T-test for $I_{K,Basal}$ difference between 2 ng and 1 ng, *p*-value = 0.001. Error bars are standard deviation

Not surprisingly, the removal of $G\alpha_{oA}$ mRNA from our suppression experiments significantly increased $I_{K,Basal}$ (Figure 3.16b). Interestingly, the 20.5.1 W7.40Trp conditions yielded the highest level of $I_{K,Total}$ ($I_{K,ACh}$ + $I_{K,Basal}$). It is unclear why the $G\alpha_{oA}$-free conditions did not produce higher $I_{K,Total}$ levels.

3.2.6.2 Batch-to-Batch cEC_{50} Variability

While removing $G\alpha_{oA}$ mRNA injections from our experimental conditions returned wild-type recovery EC_{50} values to an appropriate number, it did not reduce the overall data variability. The 20.5.0 W7.40F1Trp data set had a cell-to-cell CV of 1.03 (Figure 3.17) and a batch-to-batch CV of 1.05 (Figure 3.18); both CVs were greater than the conventional wild-type and the 20.5.2 W7.40F1Trp data sets.

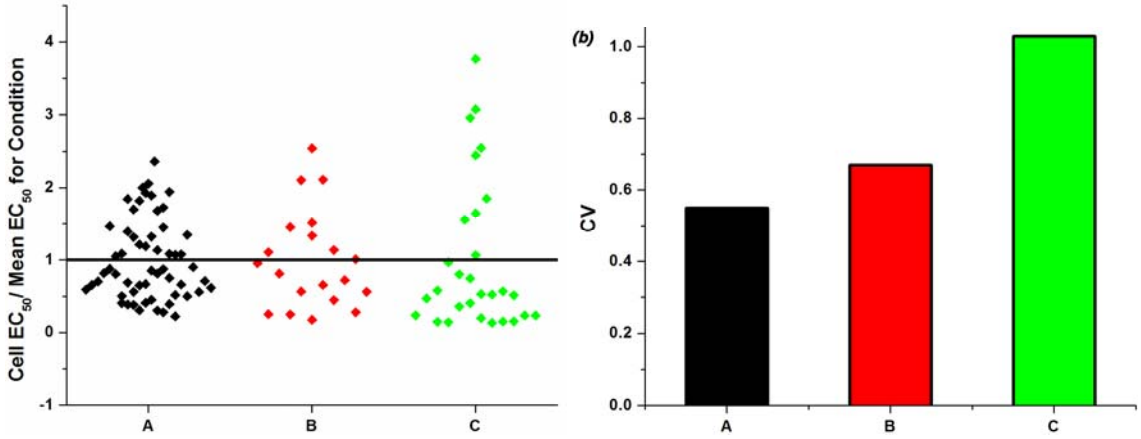

Figure 3.17. Cell-to-cell variability for conventional wild-type (A), 20.5.2 W7.40F$_1$Trp (B), and 20.5.0 W7.40F$_1$Trp (C). ***(a)*** cEC$_{50}$ values are normalized to the mean EC$_{50}$ for the condition. ***(b)*** The CVs for each condition's distribution are presented: A, CV = 0.55; B, CV = 0.68; C, CV = 1.03

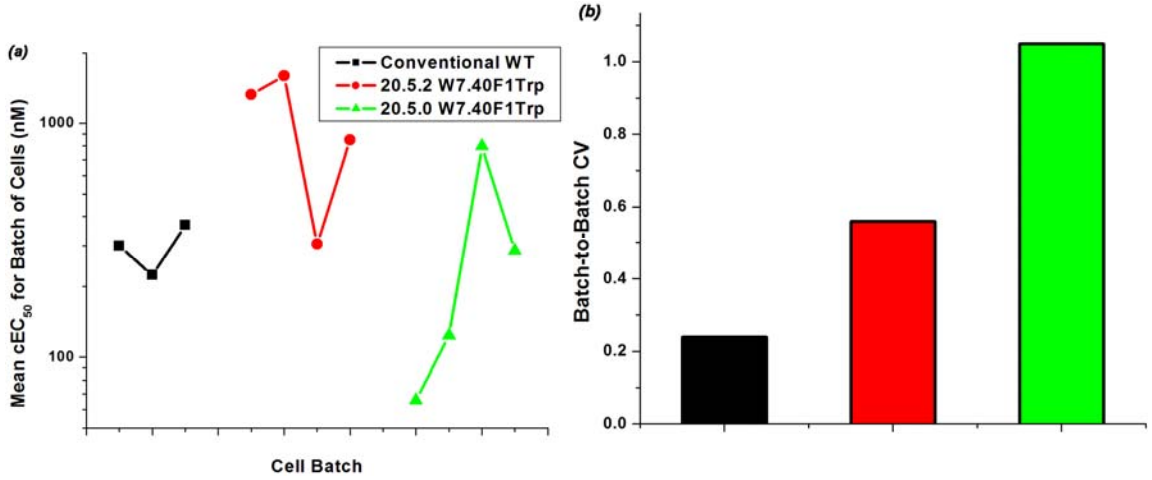

Figure 3.18. Batch-to-batch variability of conventional WT (black), 20.5.2 W7.40F$_1$Trp (red), and 20.5.0 W7.40F$_1$Trp (green). ***(a)*** Mean cEC$_{50}$ values for each cell batch of a given condition are plotted. ***(b)*** Batch-to-batch CV values for each condition are presented: conventional WT, CV = 0.24; 20.5.2 W7.40F$_1$Trp, CV = 0.56; 20.5.0 W7.40F$_1$Trp, CV = 1.05

Our next attempt to solve this variability involved varying the injection ratios of mutant M_2AChR and GIRK 1/4 mRNA. We wondered if lowering the M_2AChR : GIRK 1/4 mRNA ratio would decrease the CV of our data. Four nonsense suppression experimental conditions were compared: 20.5.0, 20.10.0, 10.10.0, and 2.5.0 had M_2AChR : GIRK 1/4 ratios of 4, 2, 1, and 0.4, respectively. A strong correlation (R = 0.98) was found between the mRNA ratio and the cell-to-cell CV (Figure 3.19). Although the 2.5.0 experimental conditions had the least variability, the expression efficiency was quite low

and irregular. We therefore decided to examine the batch-to-batch variability of sets of 10.10.0 suppression data.

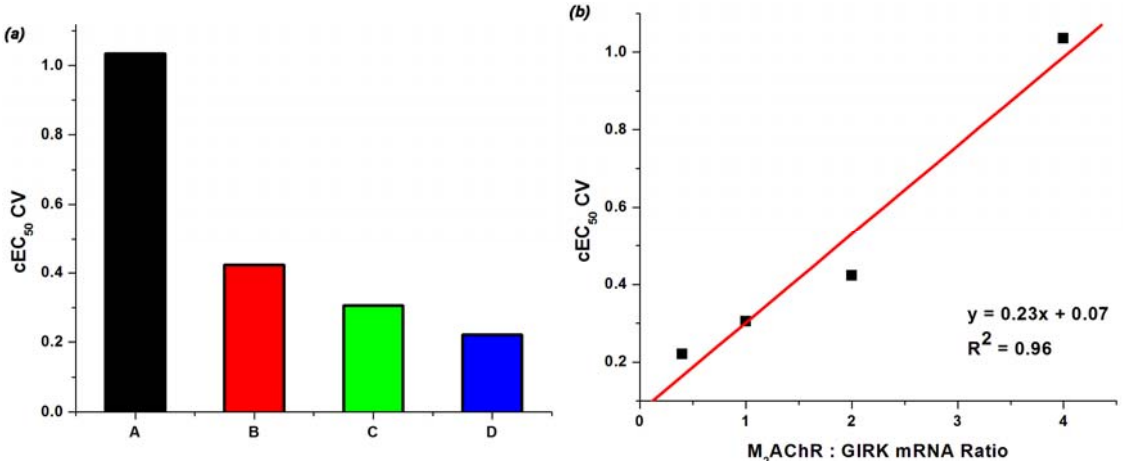

Figure 3.19. M_2AChR : GIRK mRNA injection ratio improves cell-to-cell variability. ***(a)*** Four different mRNA ratios were tested and cell-to-cell CV values were determined. (A: 20.5.0, CV = 1.03; B: 20.10.0, CV = 0.42; C: 10.10.0, CV = 0.30; D: 2.5.0, CV = 0.22). ***(b)*** A strong linear correlation between mRNA ratio and CV was found. In all four conditions, the suppression experiment measured W7.40F_1Trp EC_{50} values

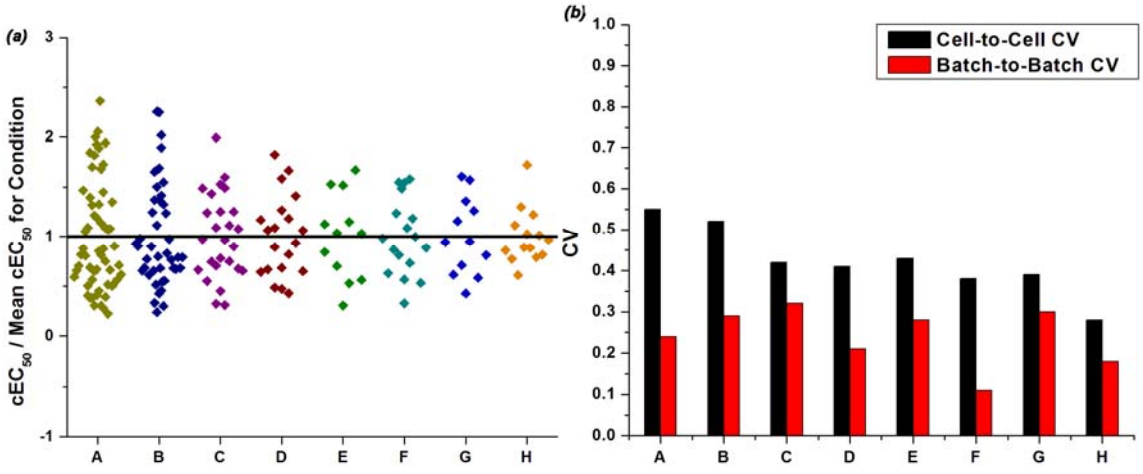

Figure 3.20. Variability of data from suppression experiments with 10.10.0 injection conditions. ***(a)*** cEC_{50} variability shown through normalizing cEC_{50} values to the mean cEC_{50} for the given condition. ***(b)*** CV values for cell and mean batch cEC_{50} values reported for each condition. (A: conventional WT, CV = 0.55 and 0.24; B: W7.40Trp, CV = 0.52 and 0.29; C: W7.40F_1Trp, CV = 0.42 and 0.32; D: W7.40F_2Trp, CV = 0.41 and 0.21; E: W7.40F_3Trp, CV = 0.43 and 0.28; F: W6.48Trp, CV = 0.38 and 0.11; G: W6.48F_2Trp, CV = 0.39 and 0.3; H: W6.48F_3Trp, CV = 0.28 and 0.18. CVs are cell-to-cell and batch-to-batch, respectively.)

Seven different sets of 10.10.0 data were obtained for mutations at two different sites in the M_2AChR, W6.48 and W7.40 (Figure 3.20). Cell-to-cell CVs for the 10.10.0 data sets ranged from 0.28 to 0.52 (the equivalent conventional CV was 0.54) and the batch-to-batch CVs ranged from 0.11 to 0.32 (the equivalent conventional CV was 0.24). The data from these seven data sets suggest that the 10.10.0 conditions are the optimal conditions for consistent nonsense suppression data in the M_2AChR-GIRK 1/4 signaling system.

3.2.6.3 Explanations of the cEC_{50} Variability

To understand the source of the variability of the 20.5.0 data, we examined three different possible mechanisms. Our first hypothesis involved expression of an endongenous oocyte GIRK subunit, GIRK5 or XIR[73]. GIRK5 is capable of forming heterotetramers with GIRK1. If the GIRK 1/5 channel had different signaling properties from the GIRK 1/4 channel, different EC_{50} values could be obtained. It is possible that different batches of cells have different levels of GIRK5 endogenous expression. To try to assess the expression levels of these channels, we injected M_2AChR mRNA with GIRK1 mRNA only. $I_{K,ACh}$ would only be produced in cells that were expressing GIRK5, because GIRK1 is incapable of forming functional homotetramers. Through three batches of oocytes, we did not once observe detectable $I_{K,ACh}$ from GIRK1-only injected cells. We concluded that our oocytes had low-to-negligible levels of endogenous GIRK5 expression, and thus GIRK5 was not the source of our variability.

Another possible explanation for batch-to-batch variability we considered was oocyte maturation-dependent differences in the expression levels of proteins in the GPCR-GIRK signaling network, such as Gβγ, β-arrestin, or GRK. Changes in the expression levels of these proteins could subtly change the signaling profile of the GPCRs. Our oocytes are harvested between maturation stages V and VI. We wondered if during this transition the levels of proteins in the signaling system fluctuate and thus cause changes in dose-response relationships.

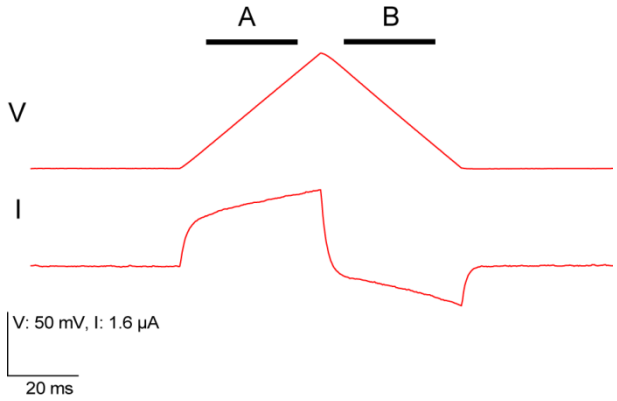

Figure 3.21. Sample of C_m measurement. First ramp begins at a holding potential of -60 mV and ends at +20 mV, while the second ramp starts at +20 mV and finishes at -60 mV. (A: samples 159 to 236; B: samples 282 to 359; ΔV = 50 mV)

To test this possibility, we first determined if cEC_{50} values changed with maturation stage. Oocytes increase in size during the transition from stage V to stage VI; this increase in cell diameter would also increase the membrane capacitance (C_m). In a collection of 10.10.0 W7.40Trp cells, we measured C_m through paired voltage ramps as described in Figure 3.21. No significant correlation was found between C_m and cEC_{50} ($R = 0.09$) and we concluded that the maturation stage did not affect cEC_{50} values.

The third and final hypothetical source of variability we tested was whether the same dose of ACh elicited the same current response throughout the course of a dose-

response relationship experiment. We spaced five test doses of 0.3 μM ACh equally throughout the ten dose series of a 10.10.0 W7.40Trp experiment (right side of Figure 3.22) and determined the percent change in response relative to the first test dose. As shown in Figure 3.22, on average, the responses increased throughout the experiment until the final test dose, where it decreased significantly. When the penultimate 10 μM dose was removed from the series of doses, we saw no significant drop in response, suggesting that the drop at test dose #5 is due to desensitization caused by two successive saturating doses of ACh. This decrease in response may also have been due to poor cell health at the end of the experiment.

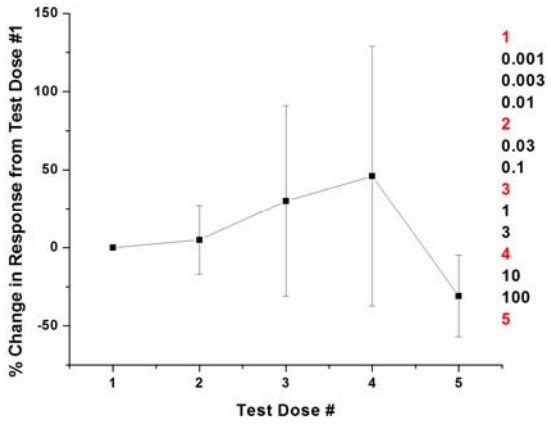

Figure 3.22. Varying responses to a test dose of ACh throughout the course of a dose-response experiment. A test pulse of 0.3 μM ACh was applied to cells at positions 1, 2, 3, 4, and 5 in the dose-response experiment (*right*). Percent change in current response is measured relative to test dose #1. Error bars are standard deviations. (% at 2 = 5 ± 20%, % at 3 = 30 ± 60%, % at 4 = 50 ± 80 %, and % at 5 = -30 ± 30 %.)

We wondered if the change in responses observed at test doses #2 through #4 could be responsible for the data variability we observed. Through an unknown biological mechanism, increased current responses during an experiment could skew dose-response relationships to higher cEC_{50} values. To investigate this possibility, we simulated dose response data using an asymmetric current change model based on the

data we had collected (see Appendix C for full description). The model we constructed started with an ideal set of dose-response data with an EC_{50} value of 140 nM; these data were then modified through current changes that were randomly sampled from current changes we recorded. cEC_{50} values from five collections of simulated data sets were not significantly different in distribution from the actual 10.10.0 W7.40Trp data we collected (Figure 3.23 and Table 3.3): both the means and variances of the simulated data were similar to the actual data. This data simulation exercise suggests that an asymmetric current change model, in which the responses to drug increase as the experiment progresses, could explain the variability in dose-response relationship data.

Table 3.3. Actual 10.10.0 W7.40Trp data and five simulated data sets[a]

	Mean cEC_{50}	**SD**	**CV**	***t*-test p[b]**	**F-test p[b]**
Actual Data	230	120	0.52	-	-
Rand1	230	150	0.64	0.9	0.2
Rand2	210	120	0.58	0.4	0.9
Rand3	230	130	0.58	0.9	0.5
Rand4	180	100	0.54	0.05	0.2
Rand5	190	90	0.47	0.07	0.05

[a]One-way ANOVA test for difference between the six data sets showed no significant difference between the sets: F-value = 1.48, df = 5,240, *p*-value = 0.2.
[b]F- and *t*-tests were performed between each simulated data set and the actual data set.

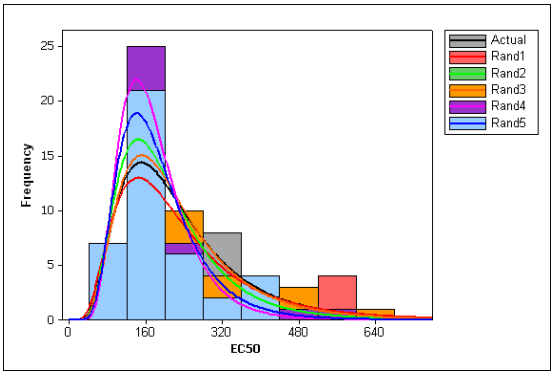

Figure 3.23. Histogram of actual 10.10.0 W7.40Trp data with five simulated data sets. Log-normal distribution fits shown. (Shape parameters are as follows: actual data: $\mu = 5.3$, $\sigma = 0.54$; Rand1: $\mu = 5.3$, $\sigma = 0.57$; Rand2: $\mu = 5.2$, $\sigma = 0.49$; Rand3: $\mu = 5.3$, $\sigma = 0.52$; Rand4: $\mu = 5.1$, $\sigma = 0.40$; Rand5: $\mu = 5.1$, $\sigma = 0.44$.)

3.2.7 Fluorinated Trp Series at W3.28, W6.48, and W7.40

With a set of suppression experiment conditions that produced stable, reliable data, we proceeded to our second goal: we began to probe aromatic residues in the M_2AChR binding site in search of a cation-π interaction. Three Trp residues were chosen as likely candidates. We chose Trp residues over Phe and Tyr residues because the calculated cation-π binding energy for the indole ring is greater than that of the other aromatic side chains (32.6 kcal/mol compared to 27.1 kcal/mol and 26.9 kcal/mol for benzene and phenol, respectively[74]). W3.28 was chosen due to its position four amino acids—approximately one turn of a helix—above the highly conserved D3.32. This position could place the indole ring in the appropriate orientation to interact with the quaternary amine of ACh as it forms an electrostatic interaction with the negatively charged Asp. W6.48 is highly conserved throughout the rhodopsin-like family of GPCRs. Rhodopsin studies have shown that the Trp side chain makes an important contact with 11-*cis*-retinal—the covalently bound agonist of rhodopsin that undergoes

photoisomerization to activate the receptor—during rhodopsin activation[25,26]. Finally, W7.40 is the most uniquely conserved residue in the aminergic class of GPCRs besides D3.32, as determined by taking all residues conserved in the aminergic class and removing residues that are also conserved in other classes of rhodopsin-like receptors[75]. Also, in the 5-HT_{2A} receptor, the W7.40A mutation completely abolishes agonist binding[76].

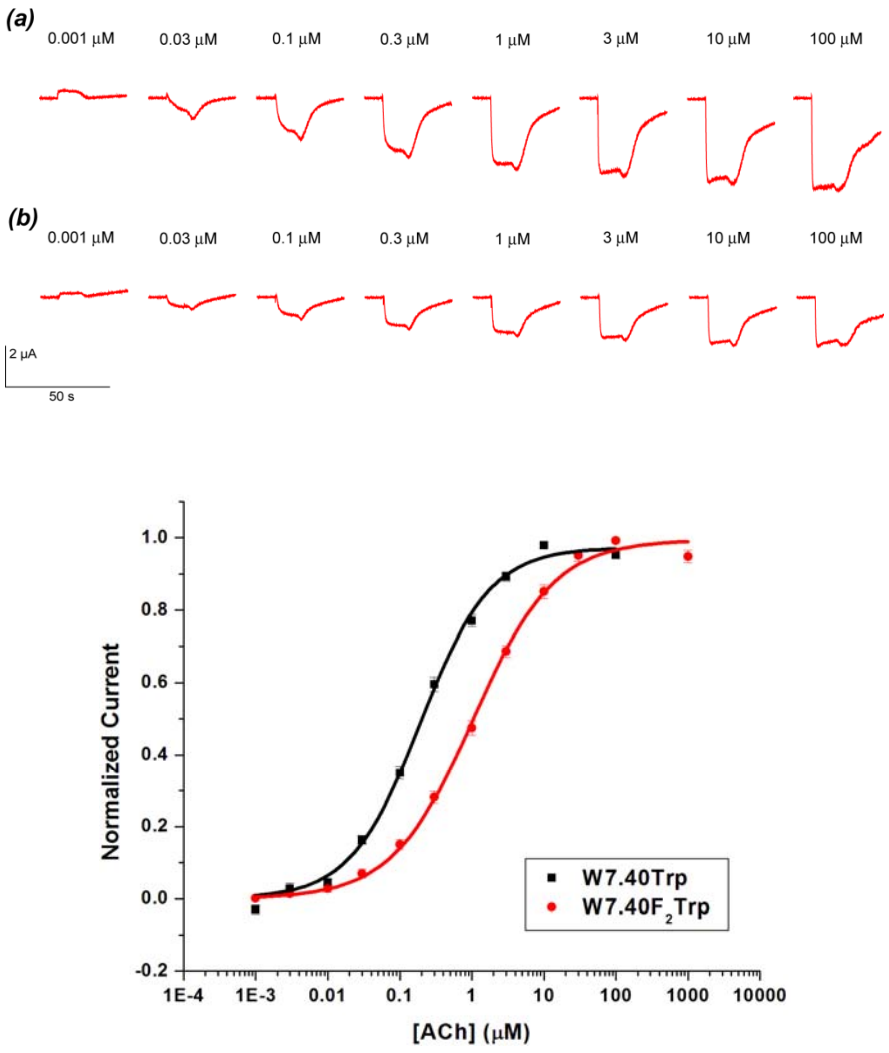

Figure 3.24. Dose-response experiment for 10.10.0 suppression conditions. *Top*: Sample traces of 10.10.0 W7.40Trp ***(a)*** and 10.10.0 W7.40F_2Trp ***(b)*** dose-response experiments. *Bottom*: Dose-response relationships fit to the Hill equation shown for the two conditions shown above

Table 3.4. F_nTrp series data at W7.40, W6.48, and W3.28[a]

	EC_{50}	n_H*	N
W7.40			
Trp	190 ± 20	0.9 ± 0.1	41
F1Trp	240 ± 9	0.9 ± 0.03	26
F2Trp	1000 ± 80	0.8 ± 0.04	20
F3Trp	170 ± 10	0.9 ± 0.05	12
W6.48			
Trp	310 ± 6	0.8 ± 0.01	17
F2Trp	1100 ± 70	0.8 ± 0.04	12
F3Trp	420 ± 30	1.1 ± 0.06	14
W3.28			
dCA	1900 ± 80	0.8 ± 0.02	12

[a]EC_{50} (nM) and n_H values are ± SEM.

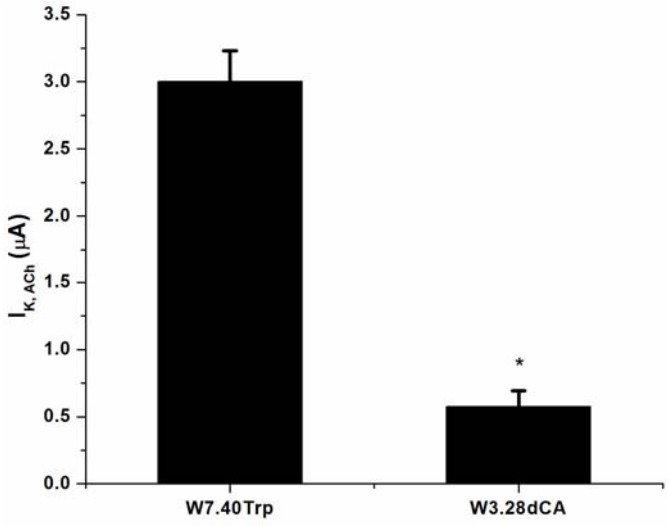

Figure 3.25. $I_{K,ACh}$ comparison between W7.40Trp and W3.28dCA. Both use 10.10.0 suppression conditions. The reaminoacylation current (W3.28dCA) was 5 times lower than the W7.40Trp currents: 3.0 ± 0.2 μA compared to 0.6 ± 0.1 μA. * *t*-test *p*-value << 0.001. Error bars are SEM

The fluorinated Trp analogs, 5-F-Trp (F_1Trp), 5,7-F_2-Trp (F_2Trp), and 5,6,7-F_3-Trp (F_3Trp), were incorporated at W7.40, while F_2Trp and F_3Trp were incorporated at W6.48. Examples of W7.40Trp and W7.40F_2Trp data are shown in Figure 3.24, and Table 3.4 summarizes the fluorinated Trp series data. Incorporation of F_2Trp produced 5- and 3.5-fold shifts in EC_{50} at W7.40 and W6.48, respectively. The other fluorinated Trp residues did not shift EC_{50} values at W7.40 or W6.48. When we performed the misacylation control experiment at W3.28 (injection of THG73-dCA), we observed definite, albeit low, $I_{K,ACh}$ (Figure 3.25). A dose-response relationship experiment on W3.28dCA yielded an EC_{50} of 1900 nM, a 10-fold increase from wild type (Table 3.4).

3.3 Discussion

3.3.1 Optimal Conditions for the Incorporation of Unnatural Amino Acids into M_2AChR

After controlling for adequate expression efficiencies and consistent dose-response relationship data, we arrived at the 10.10.0 conditions for our nonsense suppression experiments. Under these conditions, we inject 10 ng of the stop codon mutant M_2AChR mRNA, 10 ng each of GIRK1 and GIRK4 mRNA, along with 25 ng of the suppressor tRNA ligated with our amino acid of choice 48 hours prior to recording. 24 hrs later, we inject another 25 ng of tRNA and 10 ng of RGS4 mRNA.

The double injection of tRNA was necessary for high levels of expression, as measured by $I_{K,ACh}$ (Figure 3.11). RSG4 expression was used to provide more uniform, faster electrophysiology traces through the ability of the protein to accelerate both the

activation and deactivation of M_2AChR-GIRK 1/4 signaling (Figure 3.7). Injecting the RGS4 mRNA a day later than the rest of the mRNA allowed for more consistent expression of the RGS protein as observed through changes to trace kinetics. We believe that this delay in injection provides the cell's translation and membrane trafficking machinery a chance to process the M_2AChR and GIRK mRNA before expressing the RGS4 protein. Although in conventional expression experiments, co-injection of $G\alpha_{oA}$ lowered $I_{K,Basal}$ and increased $I_{K,ACh}$, we found that in nonsense suppression experiments this additional expression of $G\alpha_{oA}$ protein resulted in increased wild-type cEC_{50}s (Figure 3.16). We proposed that a large amount of $G\alpha_{oA}$ expression prematurely terminates G-protein signaling in the cell by binding free $G\beta\gamma$ released by active receptors. Finally, to avoid substantial batch-to-batch and cell-to-cell cEC_{50} variability, we found that equal-to-low M_2AChR : GIRK 1/4 mRNA injection ratios were necessary (Figure 3.20). Increasing the amount of GIRK mRNA was necessary to keep an equal ratio with M_2AChR mRNA, while still injecting enough mutant M_2AChR mRNA to allow for efficient expression of receptor. We also found that injecting cells with wild-type recovery conditions alongside cells with mutant conditions provided a good means to assess the variability of a given batch of cells.

3.3.2 What Causes cEC_{50} Variability in Suppressed M_2AChR Experiments?

By far, the biggest struggle during this project was overcoming the data variability in the nonsense suppression experiments. Perhaps it is not surprising that GPCR data would have higher variability than LGIC data. In our LGIC experiments,

drug action on the receptor of study and detectable signal were connected directly: drug binding caused a conformational change in the receptor that allowed current to pass through the cell membrane. But, in our GPCR system, multiple steps separate drug action from current signals. These steps require multiple proteins within the cell. The expression levels of some of these proteins, like GIRK, we can control, but there are others over which we have no control, like the G-protein. Other cellular pathways can intersect with these players in our signaling system. Gβγ can interact with GRKs, which can then phosphorylate our receptor to terminate signaling. Gα proteins from the $G_{i/o}$ family can also inhibit the synthesis of cAMP by AC, which can alter cAMP levels within the cell. Combine the variability caused by this spider web of cellular pathways with the variability inherent in the nonsense suppression methodology and greater fluctuations in cEC_{50}s are inevitable.

Unfortunately, the reason why the 10.10.0 injection conditions remedied the problem is not quite clear. The endogenous GIRK5 and maturation state hypotheses seemed to be strong possible explanations, but we did not detect GIRK5 expression in our cells and our measurement of maturation state (C_m) did not correlate with cEC_{50}.

The remaining explanation was provided by data from our test dose experiments (Figure 3.22). By repeating the same concentration of ACh at 5 different times during a dose-response relationship, we were able to detect a significant upward trend in responses to the same dose as the experiment progressed. Most of the changes in current responses occur around and after the midway point of the dose-response series (test dose #3). Therefore, it appeared that the first half of the dose series was unaffected by these current changes. But, in the second half, responses began to increase. This asymmetric upward

trend would effectively stretch the second half of the dose-response relationship higher than its normal state. Upon normalization, the dose-response relationship would be warped towards higher EC_{50} values. If the degree of these asymmetric current changes varied from cell to cell or batch to batch—and given the large standard deviations observed in our collected current change data, this appeared to be likely—large batch and cell variation in cEC_{50} data would be expected.

Our data simulation trials (described in detail in Appendix C), in which we utilized an asymmetric current change model on an ideal set of dose-response data, supports this hypothesis. The simulated data resembled our actual 10.10.0 W7.40Trp data in mean and variance (Figure 3.23 and Table 3.3). Unfortunately, we did not collect data on the change in responses during dose-response experiments for the 20.5.0 W7.40F1Trp trials, in which the cell-to-cell and batch-to-batch CVs were around 1. But this model suggests that data with such high variability should exhibit response changes during an experiment that are greater and even more asymmetric than the data collected in the 10.10.0 experiments. We would predict that the percent change at test dose #2 would not differ much from the 10.10.0 data, but that later test doses, #3 and #4, would show larger percent changes.

Even though this asymmetric current change model provides a source of the data variability, it does not provide a biological explanation for the variability. What cellular mechanism could cause such changes in response to the same dose of drug in the course of an experiment? The most likely explanation is some combination of changes in the receptor internalization and surface trafficking machineries. One way to test this hypothesis would be to perform a similar repeated dose experiment on non-desensitizing

M_2AChRs[77,78]. If the internalization process is the source of current changes, these mutants would eliminate the phenomenon because the non-desensitizing receptors would not be internalized. If the source of these response changes is an increase in surface trafficking over the course of an experiment, these mutations should produce larger response changes because internalization would be shut down. It is also entirely possible that response changes and their connection to equal or low M_2AChR : GIRK 1/4 mRNA injection ratios have multiple or complex causative factors. Thus, the connection may be simply phenomenological.

3.3.3 No Cation-π Interaction Site at W3.28, W6.48, or W7.40

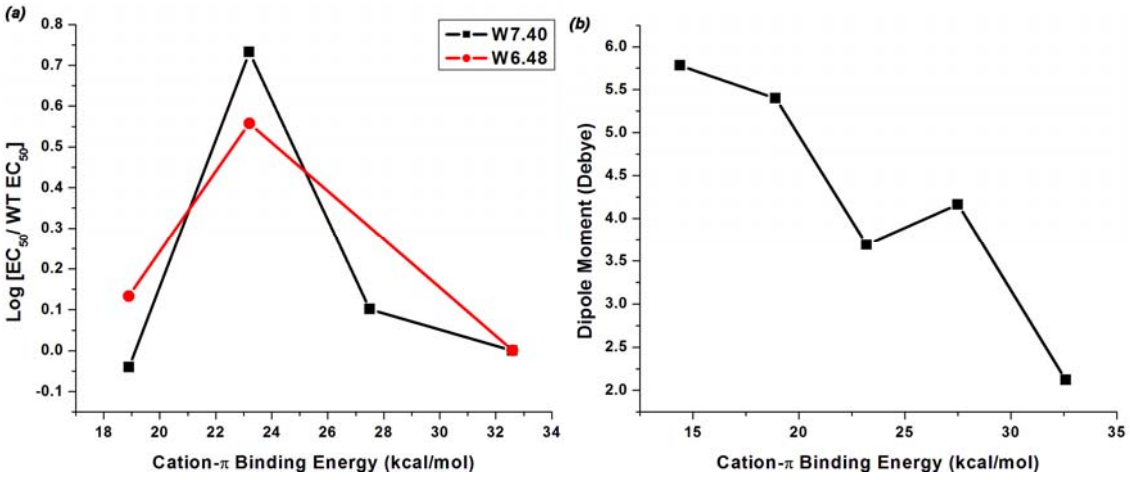

Figure 3.26. F_nTrp data analyzed in terms of cation-π binding energy and ring dipole moment. ***(a)*** Zhong Plot: calculated gas phase cation-π binding energies of fluorinated indole rings versus the log of the ratio of the F_nTrp EC_{50} and wild-type EC_{50}. ***(b)*** Plot of cation-π binding energy versus dipole moment of the same indole ring

A plot of the calculated gas-phase cation-π binding energies against a measure of the change in EC_{50} for F_nTrp mutations (a Zhong plot) at W6.48 and W7.40 does not yield the telltale linear relationship of a cation-π interaction (Figure 3.26a). We therefore

conclude that neither residue makes a conventional cation-π interaction with ACh. Also, because W3.28 failed the misacylation control experiment, we also conclude that W3.28 is not a possible site of interaction for the quaternary amine of ACh in the M_2AChR binding site. Previous experiments have shown that the amino acid incorporated by misacylated THG73 tRNA is Gln[79]. Therefore, a 10-fold shift in EC_{50} for an effective W3.28Gln mutation is not indicative of a cation-π interaction.

What causes the F_2Trp shift at W6.48 and W7.40? Fluorination of the indole ring also makes other changes to the chemistry of the aromatic moiety, beyond depleting the electrostatic potential within the ring: the dipole moment of the ring is also changed through fluorination. This change in dipole moment is not uniform, but, as shown in Figure 3.26b, the relative trend is similar enough to the cation-π binding energy trend that the F_2Trp abnormality could not be explained by a change in indole dipole moments. Partial charge on the hydrogen of the indole nitrogen is also affected by fluorination. This change follows the cation-π trend and its magnitude is negligible.

A possible explanation for the F_2Trp EC_{50} abnormality is that ACh makes a cation-π interaction with multiple aromatic residues. Incorporation of F_2Trp weakens one of these interactions. But when the weaker-binding F_3Trp is incorporated, the binding site readjusts and the quaternary amine of ACh makes contacts with the remaining cation-π sites, avoiding the significantly weakened binding residue. To test this hypothesis, multiple unnatural amino acids could be incorporated into the binding site[80]. If the quaternary amine of ACh makes contact with both W7.40 and W6.48, incorporation of

the fluorinated Trp series simultaneously at both residues should present the expected linear relationship between receptor response and cation-π binding energy.

3.3.4 Other Possible Cation-π Interaction Sites and Future M_2AChR Experiments

The recent crystal structure of the β_2AR with the inverse agonist carazolol bound provides some possible sites of interest for future studies on the M_2AChR[31]. There are nine residues found within 5 Å of the ligand that are aromatic residues in M_2AChR (Figure 3.27); we have studied three of these residues in this project. Of the six remaining aromatic residues, only one, W7.35, is a Trp. Would the quaternary amine of ACh bind to a Tyr or Phe instead of a Trp, even though Trp is the stronger cation-π binder? In previous experiments on the α7 nAChR, a cation-π interaction was discovered at Tyr 93 even though the classic Trp 149 was also present[81]. So, there is precedent for such a Tyr cation-π site. In fact, a recent model of the M_1AChR suggested that residues Y7.39, Y6.51, and Y7.43 are in the same proximity to the quaternary amine of ACh as the aromatic box residues in the nAChR[36]. An Asn at position 7.39 in the β_2AR appears to hydrogen bond with the secondary amine of carazolol in the crystal structure[31]. Therefore, there is evidence that a Tyr in the M_2AChR may serve as the anchor point for the quaternary amine of ACh.

Beyond possible cation-π interactions within the M_2AChR binding site, there are other sites of interest (Table 3.5). Tyr residues could also be studied in terms of hydrogen bonding through the incorporation MeO-Tyr and Me-Phe. Of course, D3.32 is a site of extreme interest in aminergic GPCR research. Incorporation of a nitro amino

acid at D3.32 could assess the role of the negative charge of Asp in a much more subtle manner than Ala scanning or Asn mutants. Unfortunately, the D3.32E mutation produces a significant shift in agonist affinity for carbachol at the M_2AChR[82]. Therefore, nitroalanine (Noa) would be preferable over nitrohomoalanine (Nha) for studies at this position.

```
B2 107 (3.26) EFWTSIDVLC VTASIETLCV IAVDR (3.50)
M2 97         DLWLALDYVV SNASVMNLLI ISFDR

B2 184 (EL-2) CYANETCCDF FT
M2 171        VEDGECYIQF FS

B2 196 (5.35) NQAYAIASSI VSFYVPLVIM VFVYS (5.59)
M2 183        NAAVTFGTAI AAFYLPVIIM TVLYW

B2 274 (6.36) TLGIIMGTFT LCWLPFFIVN IV    (6.57)
M2 388        TILAILLAFI ITWAPYNVMV LI

B2 306 (7.33) EVYILLNWIG YVNSGFNPLI YCRS  (7.56)
M2 420        TVWTIGYWLC YINSTINPAC YALC
```

Figure 3.27. Alignment of β_2AR and M_2AChR binding site sequences. Residues within 5 Å of the ligand in the β_2AR crystal structure are shown in red. Aromatic residues not studied in this work shown in blue; the three Trp residues studied above shown in green. EL-2 members of the conserved disulfide shown in yellow on black background

N6.52 has often been proposed to hydrogen bond with the ester moiety of ACh[32,83]. This position is a Phe in the other aminergic GPCRs that bind aromatic-based agonists, but in the non-aromatic-agonist-binding M_2AChR this residue is an Asn. The Ala mutation at N6.52 reduces agonist potency significantly[83]. Incorporation of 2-amino-4-ketopentanoic acid (Akp) at this site would provide a negligible change in sterics, but eliminate a hydrogen-bond-donating group. Noa would also eliminate a hydrogen-bond-donating group and weaken the hydrogen-bond-accepting ability of the oxygen atom. Finally, Leu would be isosteric to Asn and Akp, but incapable of being involved in any type of hydrogen bond.

Table 3.5. M_2AChR binding site residues and mutational data

Binding Site Residue	Literature Mutations[a]	Conclusion from Data or Possible UAA Mutations
W3.28[82]	**M_2AChR:** 0.3 to 5.6 fold shift in agonist affinities	W3.28dCA shows current; no cation-π
D3.32[82,84]	**M_1AChR:** Zero efficacy and 100-fold decrease in affinity **M_2AChR:** (*Glu*) 140-fold shift in carbachol affinity	Noa
Y3.33[84,85]	**M_1AChR:** 100-fold decrease in affinity and efficacy **M_3AChR:** (*Phe*) 10-fold reduction in affinity and EC_{50}	MeO-Phe, Me-Phe, F_nPhe series
W6.48[82,86]	**M_2AChR:** >10-fold shifts in agonist affinities **M_3AChR:** (*Phe*) 20-fold shift in affinity	F_nTrp series showed no cation-π
Y6.51[85,87,88]	**M_1AChR:** 10-fold decrease in affinity and 100-fold decrease in EC_{50} **M_1AChR:** (*Phe*) 10-fold decrease in potency **M_2AChR:**; (*Phe*) 100-fold decrease in potency **M_3AChR:**; (*Phe*) 10-fold decrease in potency	MeO-Phe, Me-Phe, F_nPhe series
N6.52[83]	**M_1AChR:** 10-fold decrease in potency	Akp, Noa, Leu
W7.35[89]	**M_1AChR:** 10-fold decrease in affinity	F_nTrp series
Y7.39[85,89]	**M_1AChR:** 100-fold decrease in affinity **M_3AChR: (***Phe*) 10-fold decrease in potency	MeO-Phe, Me-Phe, F_nPhe series
W7.40[76]	**5-HT_{2A}:** No binding detected	F_nTrp series showed no cation-π
Y7.43[85]	**M_3AChR: (***Phe)* 10-fold decrease in affinity and 5-fold decrease in potency	MeO-Phe, Me-Phe, F_nPhe series

[a]All mutations are Ala mutations and ligand studied is ACh, unless otherwise stated.

3.4. Materials and Methods

Molecular Biology

The genes used in these experiments were in the following plasmids: $G\alpha_{oA}$ was in a pCI plasmid, GIRK1 and GIRK4 were in pBSMXT plasmids, RGS4 was in the pcDNA3.1 plasmid, and the M_2AChR was in the pGEM3 plasmid. Plasmids were linearized with the appropriate restriction enzymes: $G\alpha_{oA}$ was linearized with ClaI, the GIRK plasmids were linearinzed with SalI, RGS4 was linearized with StuI, and the M_2AChR was linearized with HindIII. mRNA was prepared by *in vitro* runoff transcription using the Ambion (Austin, TX) T7 mMessage mMachine kit for all of the constructs except for GIRK1 and GIRK4, which required the T3 kits. For unnatural amino acid mutants, the site of interest was mutated to the amber stop codon by standard means, verified by sequencing through both strands.

Typical oocyte injection volumes were 50 nL per cell; doubly injected oocytes received 50 nL injections at each injection session. Synthetic amino acids, which were conjugated to the dinucleotide dCA and ligated to truncated 74 nt tRNA as previously described[49,90], were deprotected via a 1kW xenon lamp for 5 minutes, using WG-335 and UG-11 filters to remove the NVOC group. Injection mixture concentrations were typically made such that a 1:1 combination of a mRNA mixture solution and a volume of deprotected tRNA yielded the appropriate concentrations reported above. Wild-type recovery conditions (injecting tRNA with the native amino acid) were always injected alongside mutant conditions to control for data variability. Misacylation was controlled for at every site of unnatural amino acid incorporation through the injection of 74 nt THG73 ligated to dCA (THG73-dCA)[79].

Electrophysiology

Stage V–VI oocytes of *Xenopus laevis* were employed. Oocyte recordings were made in two-electrode voltage clamp mode using the OpusXpress^{TM} 6000A (Axon Instruments, Union City, California). Recording buffers were ND96 (96 mM NaCl, 2 mM KCl, 1 mM $MgCl_2$, 5 mM HEPES, 1.8 mM $CaCl_2$) and high potassium ringer (96 mM NaCl, 24 mM KCl, 1 mM $MgCl_2$, 5 mM HEPES, 1.8 mM $CaCl_2$). Both recording buffers were at pH 7.5. Solution flow rates were 2 ml/min during washing and pre-washing; Drug application flow rates were 4 ml/min. Initial holding potentials were -60 mV. Data were sampled at 125 Hz and filtered at 50 Hz. The ND96 pre-wash lasted 10 s; the high potassium pre-wash lasted 50 s; drug applications were 15 s in duration; the high potassium and ND96 washings were 45 s and 90 s in duration, respectively. Acetylcholine chloride was purchased from Sigma/Aldrich/RBI. All drugs were prepared in sterile ddi water for dilution into high-potassium ringer. Dose-response relations were fitted to the Hill equation, $I_{Norm} = \frac{1}{1+\left(\frac{EC_{50}}{A}\right)^{n_H}}$, where I_{Norm} is the normalized current peak at [ACh] = A, EC_{50} is the concentration of ACh that elicits a half-maximum response, and n_H is the Hill coefficient. cEC_{50} values were obtained by fitting a single cell's I_{Norm} data to the Hill equation, while EC_{50} values were obtained by averaging the I_{Norm} values for each cell at a given dose and fitting those average I_{Norm} data to the Hill equation. Statistical calculations were performed using Origin 7.0 (Origin Lab, Northhampton, MA), MiniTab (MiniTab, State College, PA), or built-in functions in Excel (Microsoft).

Wild-type recovery cEC_{50}s from a given batch of cells were compared to previous data: the cell-to-cell CV and the batch mean cEC_{50} were calculated for this comparison. This analysis was performed for each recording session to control for batch-to-batch cEC_{50} variability.

The concentration of ACh test doses was approximately equal to the EC_{50} (0.3 μM for W7.40Trp). In experiments where test doses were applied, they were inserted at positions in the dose series described in Figure 3.22. Most of the test dose experiments did not include a test dose #5, because it was believed to be uninformative. Our final dose-response experiments (the F_nTrp mutants at W7.40 and W6.48) did not include test doses.

The C_m voltage ramp experiments were performed under voltage clamp conditions[91]. Data were filtered at 1 kHz and sampled at 12.5 kHz. Each ramp trace consisted of 10 ms at -60 mV, a 10 ms ramp up to +20 mV (2 V/s), a symmetric 10 ms ramp back down to -60 mV (2 V/s), and a final 10 ms at -60 mV. Five traces per cell were collected and averaged in the Clampfit 9.0 software package (Axon Instruments, Union City, California). The averaged current traces were integrated from samples 159 to 236 for Q_A and 282 to 359 for Q_B. C_m was calculated through the equation, $C_m = \frac{Q_A+Q_B}{2\Delta V}$, where ΔV is the change in potential over the integration ranges.

3.5 References

(1) Hopkins, A. L.; Groom, C. R. *Nat Rev Drug Discov* **2002**, *1*, 727–730.
(2) Klabunde, T.; Hessler, G. *ChemBioChem* **2002**, *3*, 928–944.

(3) Lefkowitz, R. J. *Trends in Pharmacological Sciences* **2004**, *25*, 413–422.
(4) Pierce, K. L.; Premont, R. T.; Lefkowitz, R. J. *Nat Rev Mol Cell Biol* **2002**, *3*, 639–650.
(5) Kobilka, B. K. *Biochimica et Biophysica Acta (BBA)—Biomembranes* **2007**, *1768*, 794–807.
(6) Offermanns, S. *Progress in Biophysics and Molecular Biology* **2003**, *83*, 101–130.
(7) Lefkowitz, R. J.; Shenoy, S. K. *Science* **2005**, *308*, 512–517.
(8) Hermans, E. *Pharmacology & Therapeutics* **2003**, *99*, 25–44.
(9) Bunemann, M.; Frank, M.; Lohse, M. J. *Proceedings of the National Academy of Sciences* **2003**, *100*, 16077–16082.
(10) Frank, M.; Thumer, L.; Lohse, M. J.; Bunemann, M. *J. Biol. Chem.* **2005**, *280*, 24584–24590.
(11) Gales, C.; Rebois, R. V.; Hogue, M.; Trieu, P.; Breit, A.; Hebert, T. E.; Bouvier, M. *Nat Meth* **2005**, *2*, 177–184.
(12) Lachance, M.; Ethier, N.; Wolbring, G.; Schnetkamp, P. P. M.; Hebert, T. E. *Cellular Signalling* **1999**, *11*, 523–533.
(13) Neubig, R. R.; Gantzos, R. D.; Thomsen, W. J. *Biochemistry* **1988**, *27*, 2374–2384.
(14) Tian, W. N.; Duzic, E.; Lanier, S. M.; Deth, R. C. *Mol Pharmacol* **1994**, *45*, 524–531.
(15) Ellis, C. *Nat Rev Drug Discov* **2004**, *3*, 577–626.
(16) Fotiadis, D.; Jastrzebska, B.; Philippsen, A.; Müller, D. J.; Palczewski, K.; Engel, A. *Current Opinion in Structural Biology* **2006**, *16*, 252–259.
(17) Filipek, S.; Krzysko, K. A.; Fotiadis, D.; Liang, Y.; Saperstein, D. A.; Engel, A.; Palczewski, K. *Photochemical & Photobiological Sciences* **2004**, *3*, 628–638.
(18) Janetopoulos, C.; Jin, T.; Devreotes, P. *Science* **2001**, *291*, 2408–2411.
(19) Marshall, F. H. *Current Opinion in Pharmacology* **2001**, *1*, 40–44.
(20) Violin, J. D.; Lefkowitz, R. J. *Trends in Pharmacological Sciences* **2007**, *28*, 416–422.
(21) Wei, H.; Ahn, S.; Shenoy, S. K.; Karnik, S. S.; Hunyady, L.; Luttrell, L. M.; Lefkowitz, R. J. *Proceedings of the National Academy of Sciences* **2003**, *100*, 10782–10787.
(22) Whistler, J. L.; von Zastrow, M. *Proceedings of the National Academy of Sciences* **1998**, *95*, 9914–9919.
(23) Dougherty, D. A. *Chem. Rev.* **2008**, *108*, 1642–1653.
(24) Parnot, C.; Miserey-Lenkei, S.; Bardin, S.; Corvol, P.; Clauser, E. *Trends in Endocrinology and Metabolism* **2002**, *13*, 336–343.
(25) Lu, Z.L.; Saldanha, J. W.; Hulme, E. C. *Trends in Pharmacological Sciences* **2002**, *23*, 140–146.
(26) Palczewski, K.; Kumasaka, T.; Hori, T.; Behnke, C. A.; Motoshima, H.; Fox, B. A.; Trong, I. L.; Teller, D. C.; Okada, T.; Stenkamp, R. E.; Yamamoto, M.; Miyano, M. *Science* **2000**, *289*, 739–745.
(27) Filipek, S.; Teller, D. C.; Palczewski, K.; Stenkamp, R. *Annual Review of Biophysics and Biomolecular Structure* **2003**, *32*, 375–397.
(28) Ballesteros, J. A.; Shi, L.; Javitch, J. A. *Mol Pharmacol* **2001**, *60*, 1–19.

(29) Cherezov, V.; Rosenbaum, D. M.; Hanson, M. A.; Rasmussen, S. G. F.; Thian, F. S.; Kobilka, T. S.; Choi, H.J.; Kuhn, P.; Weis, W. I.; Kobilka, B. K.; Stevens, R. C. *Science* **2007**, *318*, 1258–1265.

(30) Rasmussen, S. G. F.; Choi, H.J.; Rosenbaum, D. M.; Kobilka, T. S.; Thian, F. S.; Edwards, P. C.; Burghammer, M.; Ratnala, V. R. P.; Sanishvili, R.; Fischetti, R. F.; Schertler, G. F. X.; Weis, W. I.; Kobilka, B. K. *Nature* **2007**, *450*, 383–387.

(31) Rosenbaum, D. M.; Cherezov, V.; Hanson, M. A.; Rasmussen, S. G. F.; Thian, F. S.; Kobilka, T. S.; Choi, H.J.; Yao, X.J.; Weis, W. I.; Stevens, R. C.; Kobilka, B. K. *Science* **2007**, *318*, 1266–1273.

(32) Shi, L.; Javitch, J. A. *Annual Review of Pharmacology and Toxicology* **2002**, *42*, 437–467.

(33) Archer, E.; Maigret, B.; Escrieut, C.; Pradayrol, L.; Fourmy, D. *Trends in Pharmacological Sciences* **2003**, *24*, 36–40.

(34) Hibert, M. F.; Trumpp-Kallmeyer, S.; Bruinvels, A.; Hoflack, J. *Mol Pharmacol* **1991**, *40*, 8–15.

(35) Jöhren, K.; Höltje, H.D. *Journal of Computer-Aided Molecular Design* **2002**, *16*, 795–801.

(36) Peng, J. Y.; Vaidehi, N.; Hall, S. E.; Goddard, W. A., III. *ChemMedChem* **2006**, *1*, 878–890.

(37) Kalani, M. Y. S.; Vaidehi, N.; Hall, S. E.; Trabanino, R. J.; Freddolino, P. L.; Kalani, M. A.; Floriano, W. B.; Kam, V. W. T.; Goddard, W. A., III. *Proceedings of the National Academy of Sciences* **2004**, *101*, 3815–3820.

(38) Selent, J.; Brandt, W.; Pamperin, D.; Göber, B. *Bioorganic & Medicinal Chemistry* **2006**, *14*, 1729–1736.

(39) Vistoli, G.; Pedretti, A.; Dei, S.; Scapecchi, S.; Marconi, C.; Romanelli, M. N. *Bioorganic & Medicinal Chemistry* **2008**, *16*, 3049–3058.

(40) Jacobsen, J. *Current Topics in Medicinal Chemistry* **2002**, *2*, 343–352.

(41) Raedler, T. J.; Bymaster, F. P.; Tandon, R.; Copolov, D.; Dean, B. *Mol Psychiatry* **2006**, *12*, 232–246.

(42) Eglen, R. M.; Choppin, A.; Watson, N. *Trends in Pharmacological Sciences* **2001**, *22*, 409–414.

(43) Beene, D. L.; Brandt, G. S.; Zhong, W.; Zacharias, N. M.; Lester, H. A.; Dougherty, D. A. *Biochemistry* **2002**, *41*, 10262–10269.

(44) Beene, D. L.; Price, K. L.; Lester, H. A.; Dougherty, D. A.; Lummis, S. C. R. *J. Neurosci.* **2004**, *24*, 9097–9104.

(45) Cashin, A. L.; Petersson, E. J.; Lester, H. A.; Dougherty, D. A. *J. Am. Chem. Soc.* **2005**, *127*, 350–356.

(46) Cashin, A. L.; Torrice, M. M.; McMenimen, K. A.; Lester, H. A.; Dougherty, D. A. *Biochemistry* **2007**, *46*, 630–639.

(47) Dougherty, D. A. *Current Opinion in Chemical Biology* **2000**, *4*, 645–652.

(48) Dougherty, D. A. *J. Org. Chem.* **2008**, *73*, 3667–3673.

(49) England, P. M.; Lester, H. A.; Dougherty, D. A. *Tetrahedron Letters* **1999**, *40*, 6189–6192.

(50) England, P. M.; Zhang, Y.; Dougherty, D. A.; Lester, H. A. *Cell* **1999**, *96M1 nAChR*, 89–98.

(51) Kearney, P. C.; Nowak, M. W.; Zhong, W.; Silverman, S. K.; Lester, H. A.; Dougherty, D. A. *Mol Pharmacol* **1996**, *50*, 1401–1412.
(52) Li, L. T.; Zhong, W. G.; Zacharias, N.; Gibbs, C.; Lester, H. A.; Dougherty, D. A. *Chemistry & Biology* **2001**, *8*, 47–58.
(53) Lummis, S. C. R.; Beene, D. L.; Lee, L. W.; Lester, H. A.; Broadhurst, R. W.; Dougherty, D. A. *Nature* **2005**, *438*, 248–252.
(54) Lummis, S. C. R.; L. Beene, D.; Harrison, N. J.; Lester, H. A.; Dougherty, D. A. *Chemistry & Biology* **2005**, *12*, 993–997.
(55) McMenimen, K. A.; Petersson, E. J.; Lester, H. A.; Dougherty, D. A. *ACS Chem. Biol.* **2006**, *1*, 227–234.
(56) Mu, T. W.; Lester, H. A.; Dougherty, D. A. *J. Am. Chem. Soc.* **2003**, *125*, 6850–6851.
(57) Nowak, M. W.; Gallivan, J. P.; Silverman, S. K.; Labarca, C. G.; Dougherty, D. A.; Lester, H. A.; Conn, P. M. *Methods in Enzymology* **1998**, *293*, 504–529.
(58) Padgett, C. L.; Hanek, A. P.; Lester, H. A.; Dougherty, D. A.; Lummis, S. C. R. *J. Neurosci.* **2007**, *27*, 886–892.
(59) Petersson, E. J.; Choi, A.; Dahan, D. S.; Lester, H. A.; Dougherty, D. A. *J. Am. Chem. Soc.* **2002**, *124*, 12662–12663.
(60) Zhong, W.; Gallivan, J. P.; Zhang, Y.; Li, L.; Lester, H. A.; Dougherty, D. A. *PNAS* **1998**, *95*, 12088–12093.
(61) Ivanina, T.; Rishal, I.; Varon, D.; Mullner, C.; Frohnwieser-Steinecke, B.; Schreibmayer, W.; Dessauer, C. W.; Dascal, N. *J. Biol. Chem.* **2003**, *278*, 29174–29183.
(62) Krapivinsky, G.; Krapivinsky, L.; Wickman, K.; Clapham, D. E. *J. Biol. Chem.* **1995**, *270*, 29059–29062.
(63) Mark, M. D.; Herlitze, S. *European Journal of Biochemistry* **2000**, *267*, 5830–5836.
(64) Kofuji, P.; Davidson, N.; Lester, H. A. *Proceedings of the National Academy of Sciences* **1995**, *92*, 6542–6546.
(65) Sadja, R.; Alagem, N.; Reuveny, E. *Neuron* **2003**, *39*, 9–12.
(66) Zhang, Q. L.; Pacheco, M. A.; Doupnik, C. A. *Journal of Physiology—London* **2002**, *545*, 355–373.
(67) Dascal, N.; Schreibmayer, W.; Lim, N. F.; Wang, W.; Chavkin, C.; DiMagno, L.; Labarca, C.; Kieffer, B. L.; Gaveriaxu-Ruff, C.; Trollinger, D.; Lester, H. A.; Davidson, N. *Proceedings of the National Academy of Sciences* **1993**, *90*, 10235–10239.
(68) Sakmann, B.; Noma, A.; Trautwein, W. *Nature* **1983**, *303*, 250–253.
(69) Zhong, W. G.; Gallivan, J. P.; Zhang, Y. O.; Li, L. T.; Lester, H. A.; Dougherty, D. A. *Proceedings of the National Academy of Sciences of the United States of America* **1998**, *95*, 12088–12093.
(70) Doupnik, C. A.; Lim, N. F.; Kofuji, P.; Davidson, N.; Lester, H. A. *J. Gen. Physiol.* **1995**, *106*, 1–23.
(71) Rishal, I.; Porozov, Y.; Yakubovich, D.; Varon, D.; Dascal, N. *J. Biol. Chem.* **2005**, *280*, 16685–16694.
(72) Doupnik, C. A.; Davidson, N.; Lester, H. A.; Kofuji, P. *Proceedings of the National Academy of Sciences* **1997**, *94*, 10461–10466.

(73) Hedin, K. E.; Lim, N. F.; Clapham, D. E. *Neuron* **1996**, *16*, 423–429.
(74) Ma, J. C.; Dougherty, D. A. *Chem. Rev.* **1997**, *97*, 1303–1324.
(75) Huang, E. S. *Protein Sci* **2003**, *12*, 1360–1367.
(76) Roth, B. L.; Shoham, M.; Choudhary, M. S.; Khan, N. *Mol Pharmacol* **1997**, *52*, 259–266.
(77) Pals-Rylaarsdam, R.; Hosey, M. M. *J. Biol. Chem.* **1997**, *272*, 14152–14158.
(78) Pals-Rylaarsdam, R.; Xu, Y.; Witt-Enderby, P.; Benovic, J. L.; Hosey, M. M. *J. Biol. Chem.* **1995**, *270*, 29004–29011.
(79) Rodriguez, E. A.; Lester, H. A.; Dougherty, D. A. *RNA* **2007**, *13*, 1703–1714.
(80) Rodriguez, E. A.; Lester, H. A.; Dougherty, D. A. *Proc. Natl. Acad. Sci.* **2006**, *103*, 8650–8655.
(81) Xiu, X. California Institute of Technology, 2007.
(82) Heitz, F.; Holzwarth, J. A.; Gies, J. P.; Pruss, R. M.; Trumpp-Kallmeyer, S.; Hibert, M. F.; Guenet, C. *European Journal of Pharmacology* **1999**, *380*, 183–195.
(83) Huang, X.P.; Nagy, P. I.; Williams, F. E.; Peseckis, S. M.; Messer, W. S., Jr. *Br J Pharmacol* **1999**, *126*, 735–745.
(84) Lu, Z.L.; Hulme, E. C. *J. Biol. Chem.* **1999**, *274*, 7309–7315.
(85) Wess, J.; Gdula, D.; Brann, M. R. *Embo Journal* **1991**, *10*, 3729–3734.
(86) Wess, J.; Nanavati, S.; Vogel, Z.; Maggio, R. *Embo Journal* **1993**, *12*, 331–338.
(87) Vogel, W. K.; Sheehan, D. M.; Schimerlik, M. I. *Mol Pharmacol* **1997**, *52*, 1087–1094.
(88) Ward, S. D. C.; Curtis, C. A. M.; Hulme, E. C. *Mol Pharmacol* **1999**, *56*, 1031–1041.
(89) Matsui, H.; Lazareno, S.; Birdsall, N. J. *Mol Pharmacol* **1995**, *47*, 88–98.
(90) Nowak, M. W.; Gallivan, J. P.; Silverman, S. K.; Labarca, C. G.; Dougherty, D. A.; Lester, H. A. *Ion Channels, Pt. B* **1998**, *293*, 504–529.
(91) Schmitt, B. M.; Koepsell, H. *Biophys. J.* **2002**, *82*, 1345–1357.